Optical brain imaging *in vivo*: techniques and applications from animal to man

Elizabeth M. C. Hillman
Columbia University
Laboratory for Functional Optical Imaging
Department of Biomedical Engineering
351ET, 1210 Amsterdam Avenue
New York, New York 10027
E-mail: eh2245@columbia.edu

Abstract. Optical brain imaging has seen 30 years of intense development, and has grown into a rich and diverse field. *In-vivo* imaging using light provides unprecedented sensitivity to functional changes through intrinsic contrast, and is rapidly exploiting the growing availability of exogenous optical contrast agents. Light can be used to image microscopic structure and function *in vivo* in exposed animal brain, while also allowing noninvasive imaging of hemodynamics and metabolism in a clinical setting. This work presents an overview of the wide range of approaches currently being applied to *in-vivo* optical brain imaging, from animal to man. Techniques include multispectral optical imaging, voltage sensitive dye imaging and speckle-flow imaging of exposed cortex, *in-vivo* two-photon microscopy of the living brain, and the broad range of noninvasive topography and tomography approaches to near-infrared imaging of the human brain. The basic principles of each technique are described, followed by examples of current applications to cutting-edge neuroscience research. In summary, it is shown that optical brain imaging continues to grow and evolve, embracing new technologies and advancing to address ever more complex and important neuroscience questions. [DOI: 10.1117/1.2789693]

Keywords: optical imaging; two-photon microscopy; near-infrared spectroscopy; diffuse optical tomography; neuroimaging; neurovascular coupling.

Paper 07027SSR received Jan. 18, 2007; revised manuscript received Apr. 26, 2007; accepted for publication May 15, 2007; published online Nov. 1, 2007.

1 Introduction

30 years ago, Jöbsis demonstrated that it was possible to measure blood and tissue oxygenation changes in the brain of a cat using near-infrared (NIR) light.[1] Since then, optical brain imaging has grown into a rich and diverse field, encompassing both basic science and clinical applications that exploit the unique properties of light to image the brain.

There are significant benefits to using light to image living tissue. Most importantly, light can provide exquisite sensitivity to functional changes, either via intrinsic changes in absorption, fluorescence, or scatter, or through the use of extrinsic contrast. Oxy- and deoxyhemoglobin (HbO_2 and HbR) are the most widely measured intrinsic chromophores, alongside cytochromes and metabolites, which have distinctive absorption or fluorescence characteristics. Absorbing and fluorescent dyes, as well as cutting-edge transgenic methods, can also provide highly specific optical contrast enhancement, often capable of actively reporting functional parameters such as changes in membrane potential or ion concentrations.[2–5] A continuing rich supply of new optical contrast agents is also anticipated, particularly since unlike contrast agents for most other imaging modalities, optical contrast is often a natural feature of many small, biocompatible molecules. Additional advantages of optical imaging include its use of nonionizing radiation, and that instruments are generally inexpensive compared to other clinical imaging modalities.

The major challenge of optical imaging is to overcome the effects of light scattering, which limits penetration depth and achievable imaging resolution. "Optical imaging" therefore encompasses a very wide range of measurement techniques, each using different methods to overcome the effects of scatter. These range from laser scanning microscopy of submicron structures, to diffuse optical tomography of large volumes of tissue.

Functional brain imaging has also seen dramatic growth in recent years, impacted significantly by the availability of functional magnetic resonance imaging (fMRI) since 1990.[6–9] As a result, new applications of functional brain imaging in humans and animals are continually being established, including neurosurgical planning, the investigation of the physiological basis of neurological diseases such as epilepsy, Alzheimer's, and stroke, the development of diagnostic methods, drugs, treatments, and interventions, and the study of cognitive and perceptual responses and developmental changes.[9] Positron emission tomography (PET) and x-ray

Address all correspondence to Elizabeth M.C. Hillman, Biomedical Engineering, Columbia University, 351L Engineering Terrace - 1210 Amsterdam Ave, New York, NY 10027; Tel.: 212–854–2788; Fax: 212 8548725; E-mail: eh2245@columbia.edu

1083-3668/2007/12(5)/051402/28/$25.00 © 2007 SPIE

computed tomography (x-ray CT) are also valuable and established tools for brain imaging.

The obvious advantage of optical imaging over other modalities is reduced cost and infrastructure requirements (such as shielded rooms and synchrotrons). However, a much more important distinction is that optical imaging offers such a broad range of contrast mechanisms. While fMRI, PET, and x-ray CT are more established clinical modalities, all suffer from limited functional contrast. For example, to visualize regions of the brain exhibiting functional changes in response to stimuli, fMRI typically exploits the blood oxygen level dependent (BOLD) signal, widely thought to correlate with HbR concentration. However, a BOLD increase (an HbR decrease) may correspond to an increase in oxygenation, *or* a decrease in blood volume. Newer fMRI methods such as arterial spin labeling (ASL) can provide measures of flow, and intravenous contrast agents such as monocrystalline iron oxide nanocompounds (MION) can allow cerebral blood volume (CBV) changes to be observed.[10,11] However, these measurements cannot easily be acquired simultaneously, and only the combination of these methods can provide insight into the true hemodynamic responses and oxygenation dynamics in the brain.[12]

PET is performed using contrast agents such as 2-fluoro-2-deoxy-D-glucose containing radioactive isotopes of carbon, nitrogen, fluorine, or oxygen. Oxygen and glucose utilization in the brain can be imaged via the localization of these isotopes. However, resolution is typically poor, data acquisition is slow (and hence dynamics cannot be readily evaluated), contrast agents must be manufactured locally prior to each scan, and radioactive dose limits its use in certain patient populations, often including infants. X-ray CTs (as well as structural MRI) have excellent spatial resolution and can be used to detect morphological changes in the brain, for example following stroke or to delineate tumors. However, CT typically cannot elicit information about the function of the tissue, and so potentially reversible changes preceding structural changes cannot be detected. Therefore, the real advantage of optical imaging over these techniques is its ability to detect and image a wide range of functional parameters.

For clinical applications, noninvasive optical imaging can provide complimentary information to other modalities such as fMRI and provide a low-cost alternative in some cases. This is in addition to serving populations often unable to receive MRI or PET scans such as young infants or the critically ill. Clinical optical brain imaging is generally noninvasive and uses near-infrared (NIR) light to obtain improved penetration through the scalp, skull, and brain [see Fig. 1(a)].

In addition, optical brain imaging is finding widespread applications as a research tool for both clinical and animal studies of basic brain function and diseases. Still, so little is known about the way that the normal brain functions, in part due to the difficulties of measuring such a complex organ without disturbing or damaging its *in-vivo* function. Optical imaging allows the living brain to be closely observed, and many functional interactions and changes to be investigated over many length scales. The effects of pathologies and treatments can also be readily investigated using fairly basic optical imaging tools. In animals, it is also relatively simple to expose the cortex, allowing high-resolution direct optical imaging of the brain's surface. Extrinsic dyes and visible wavelengths can also be used [see Fig. 1(b)].

In summary, optical imaging's key advantage is the ability to measure a range of functional contrast, can readily be exploited in functional brain imaging via a wide range of approaches, from animal studies of the intricate cellular mechanisms of normal and diseased brain, to *in-vivo* noninvasive clinical brain imaging.

In this review, we describe a variety of optical imaging approaches to functional brain imaging. The basic principles of each technique are summarized, followed by examples of use for *in-vivo* brain imaging. Section 2 details the use of optical techniques for exposed cortex imaging. Section 3 describes noninvasive clinical optical imaging of the living brain.

2 Exposed-Cortex Imaging and Microscopy

The use of optical imaging in animal studies is widespread. Animal imaging has become more than just a step toward clinical diagnostic imaging, but a tool with which to learn more about the basic mechanisms of brain function as well as disease processes and the effects of treatments. These findings can be utilized in their own right to aid in the development of drugs and treatment. They can also contribute to the interpretation of results from other imaging modalities such as fMRI. Recent applications of animal imaging have included studies of stroke (acute and chronic),[13] Alzheimer's disease,[14] migraine,[15] epilepsy,[16] the effects of cocaine,[17] and the mechanisms of neurovascular coupling.[18,19]

Imaging animals rather than humans provides significantly more flexibility, since preparations can be much more controlled and diseases and treatments can be systematically compared. Extrinsic dyes and cross-validation techniques such as electrophysiology can be utilized and developed without the need for clinical regulatory approval. The adverse effects of light scattering worsen as the size of the tissue being interrogated increases. Imaging smaller animals therefore also offers significant technical advantages, allowing higher resolution imaging and improved sensitivity and quantitation. For very high resolution imaging, the cortex can be surgically exposed, allowing direct optical imaging of the brain's surface with only minimal disturbance to normal brain activity. Exposed cortex optical imaging is highly versatile, and most commonly performed in animals, although it has also been performed on the human brain, for example, during epilepsy surgery.[20–22]

Next, we provide an overview of the most established exposed-cortex, *in-vivo* optical neuroimaging techniques ranging from 2-D and 3-D macroscopic imaging to microscopic *in-vivo* imaging using two-photon microscopy. Basic principles and methods are first described, followed by specific examples of neuroimaging applications.

2.1 *Macroscopic Optical Imaging of Exposed Cortex in Two Dimensions*

2.1.1 *Experimental method*

During surgical preparation for exposed-cortex imaging, the animal (commonly mouse, rat, cat, or primate) is anesthetized while the scalp is retracted and the skull is gently thinned over the brain area of interest. In some cases, this piece of skull

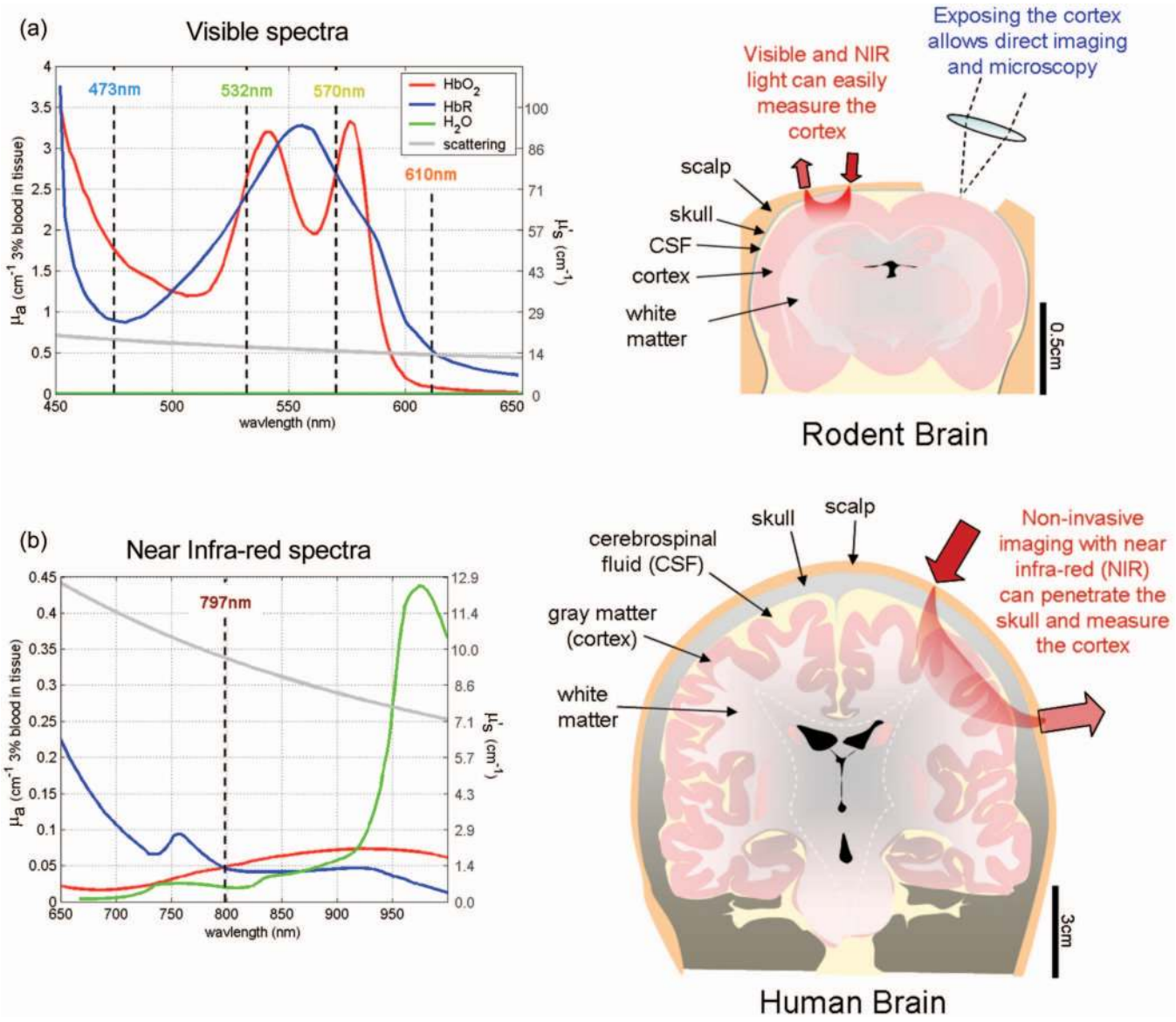

Fig. 1 Intrinsic chromophores and structures of the brain. (a) For small animal imaging, it is possible to use visible light to look at oxygenation-dependent hemoglobin absorption (as well as exogenous absorbing and fluorescing dyes). The cortex can be exposed and imaged at high resolution, or imaged through the intact skull and scalp at lower resolution. (b) For human brain imaging, near-infrared light will penetrate more readily through the scalp and skull to sample the brain thanks to lower scatter and absorption. The human brain has a more complex convoluted structure compared to lower mammals. Spectra: major chromophores in brain are oxy- and deoxyhemoglobin and water (lipid is omitted here). For generation of these spectra: water content is assumed to be 90% (quoted value in newborn brain, 71 to 85% in adult brain[34]). Hemoglobin absorption is shown assuming 2-mM concentration of hemoglobin in blood and 3% content of blood in tissue (60 mM in tissue[34]) calculated from spectra.[257] HbR spectrum represents 3% fully deoxygenated blood in tissue. Scatter spectrum is approximate using: $\mu's = A\lambda^{-b}$, where $A = 1.14 \times 10^{-7}$ m and $b = 1.3$.[228]

may be removed to provide a direct view of an area of the brain's surface. In mice, the brain can often be visualized without even thinning the skull. Methods have been carefully developed to ensure that normal brain function is not affected by these approaches. Most often, the animal will remain anesthetized during measurements.[23] In some cases, however, a permanent window can be surgically implanted and the animals can survive for over a year while an area of their brain is accessible for repeated direct optical imaging.[14,24]

Imaging of pathologies requires only that the animal be anesthetized. Images during acute interventions, such as administration of drugs or introduction of a stroke, must be carefully synchronized with image acquisition. While the brain's functional response to stimulus is being studied, a carefully controlled stimulus is presented during imaging. Such stimuli may include visual (e.g., showing patterns or pictures), somatosensory (e.g., electrical or tactile stimulation of the whiskers or forepaw), or auditory stimuli (different frequencies and amplitudes). Stimuli may be repeated in regular blocks, or presented in a randomized pattern.[18,25] Data are usually shown as the average response to multiple stimulus repetitions to obtain

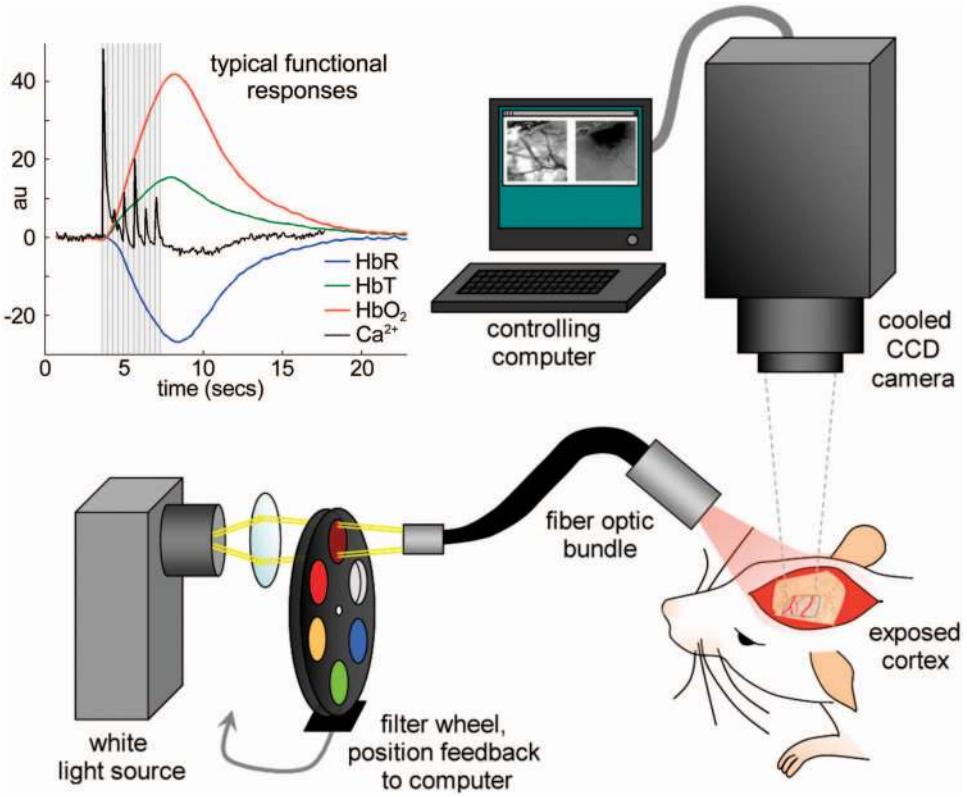

Fig. 2 A typical setup for camera-based imaging of the exposed cortex. Inset shows typical hemodynamic and calcium-sensitive responses in rat somatosensory cortex to ~1-mA forepaw stimulus delivered in 3 msec pulses at 3 Hz for 4 sec.

better signal to noise (where noise includes normal background physiological variations).

2.1.2 *Basic principles: two-dimensional camera-based imaging*

2-D camera-based imaging of the exposed cortex is the most simple of optical imaging techniques and is often referred to as "optical imaging" in the neuroscience literature. We describe three approaches to 2-D imaging of the cortex: 1. intrinsic signal or hyperspectral imaging of oxy- and deoxyhemoglobin dynamics; 2. imaging of extrinsic voltage sensitive dyes (providing sensitivity to neuronal activity); and 3. speckle flow imaging, capable of imaging the blood flow dynamics in the superficial cortex.

Two-dimensional intrinsic and hyperspectral imaging. Figure 2 shows a typical setup for 2-D hyperspectral imaging of exposed rat cortex. This neuroimaging approach relies on the distinctive absorption spectra of oxy- and deoxyhemoglobin (HbO_2 and HbR) as shown in Fig. 1(a). The hemoglobin in blood is the most significant absorber in the brain at visible and NIR wavelengths, and functional activity in the brain results in changes in blood flow, blood volume, and oxygenation.[26]. Blood delivers oxygen to tissues by locally converting HbO_2 to HbR, so changes in the oxygenation state of blood correspond to changes in the relative concentrations of HbO_2 and HbR. Consequently, variations in the amount and oxygenation state of hemoglobin modulate the absorption properties of the brain. By simply shining light into the exposed cortex and taking pictures with a camera, the hemodynamic response to stimulus can be readliy observed. Further, since HbR and HbO_2 have different absorption spectra [see Figs. 1(a) and 1(b)], measurements with different wavelengths of light can produce images that are preferentially sensitive to changes in the concentration of either HbO_2 or HbR. At isobestic points, where the HbR and HbO_2 absorption is the same (e.g., ~500, 530, 570, and 797 nm), changes in total hemoglobin concentration ($HbT = HbR + HbO_2$) can be measured independently of changes in blood oxygenation.

Early approaches to optical imaging of the exposed cortex referred to "intrinsic signal" imaging, and often used illumination at an isobestic point to examine localized changes in tissue HbT.[27] By adding a second wavelength (often 610 nm), researchers were able to investigate oximetric changes in addition to changes in HbT.[28,29] Since HbO_2 absorption at 610 nm is low (around 16% of the absorption of HbR), changes in absorption at 610 nm are largely attributed to, and interpreted as, changes in HbR. However, it should be noted that even though HbO_2 absorption at 610 nm is lower than that of HbR, HbO_2 changes can interfere with and distort inference of HbR concentration changes from measurements at 610 nm.

To calculate the actual changes in concentration of HbO_2, HbR, and HbT, the absorption of the brain must be measured at two or more wavelengths (hyperspectral imaging). In some cases, multiple wavelengths across the visible spectrum are used. This is typically achieved by synchronizing rapid camera acquisition with a filter wheel in front of a white light

source, as shown in Fig. 2.[30,31] Full spectra of the reflectance changes along a single line on the cortex have also been used to provide a more detailed spectral picture of the changes occurring during functional activation.[32,33]

Calculation of hemoglobin concentrations from such measurements is not trivial, as the effects of scattering must be considered, and then data must be combined with the known spectra for HbO_2 and HbR to deduce the concentration changes corresponding to the measurements. In this case, we assume that scattering in the brain does not change significantly during the hemodynamic response. (Note that the following approach is also applied to noninvasive clinical optical topography, as is discussed in Sec. 2). The basis of this approach is the modified Beer-Lambert law,[34] which states that:

$$\frac{I}{I_0} = \exp(-\mu_a \mathrm{DPF}x + G), \tag{1}$$

where I is the detected intensity, I_0 is the incident intensity, DPFx is the mean pathlength traveled by light in the tissue (a function of baseline scattering and absorbing properties), G is a geometry-dependent factor, and μ_a is the absorption coefficient of the tissue as given by Beer's law:

$$\mu_a = \sum_n \xi_n c_n, \tag{2}$$

i.e., the absorption coefficient is a linear sum of the absorption of the n chromophores in the tissue, where ξ_n is the wavelength-dependent specific absorption coefficient of a particular chromophore (e.g., the HbO_2 absorption spectrum) and c_n is its concentration. Note that "differential pathlength factor" (DPF) is a term used to describe the approximate multiplicative increase in pathlength experienced by a photon traveling in a scattering medium between two points a linear distance x apart. Thus, the true pathlength is DPFx.

I_0 may be spatially varying and difficult to accurately determine. G is also very difficult to quantify. Therefore, it is common to consider *changes* in detected signal relative to an initial time point $t=0$ or a reference state:

$$\ln\left[\frac{I(t)}{I(t_0)}\right] = -[\mu_a(t) - \mu_a(t_0)]\mathrm{DPF}x$$

$$\Delta \ln(I) = -\Delta\mu_a \mathrm{DPF}x. \tag{3}$$

If measurements at two wavelengths (λ_1 and λ_2) are acquired, it is possible to use these differential measurements to determine the changes in HbO_2 and HbR concentration occurring relative to time $t=t_0$ using:

$$\Delta \ln(I)_{\lambda 1} = -(\xi_{\mathrm{HbO}_2,\lambda 1}\Delta c_{\mathrm{HbO}_2} + \xi_{\mathrm{HbR},\lambda 1}\Delta c_{\mathrm{HbR}})\mathrm{DPF}x_{\lambda 1}$$

$$\Delta \ln(I)_{\lambda 2} = -(\xi_{\mathrm{HbO}_2,\lambda 2}\Delta c_{\mathrm{HbO}_2} + \xi_{\mathrm{HbR},\lambda 2}\Delta c_{\mathrm{HbR}})\mathrm{DPF}x_{\lambda 2}. \tag{4}$$

Where more than two wavelengths are available, HbO_2 and HbR can be calculated using a linear model:

$$\begin{pmatrix} \Delta \ln(I)_{\lambda 1} \\ \Delta \ln(I)_{\lambda 1} \\ \vdots \\ \Delta \ln(I)_{\lambda n} \end{pmatrix} = \begin{pmatrix} \mathrm{DPF}x_{\lambda 1}\xi_{\mathrm{HbO}_2,\lambda 1} & \mathrm{DPF}x_{\lambda 1}\xi_{\mathrm{HbR}_2,\lambda 1} \\ \mathrm{DPF}x_{\lambda 2}\xi_{\mathrm{HbO}_2,\lambda 2} & \mathrm{DPF}x_{\lambda 2}\xi_{\mathrm{HbR}_2,\lambda_2} \\ \vdots & \vdots \\ \mathrm{DPF}x_{\lambda n}\xi_{\mathrm{HbO}_2,\lambda n} & \mathrm{DPF}x_{\lambda n}\xi_{\mathrm{HbR}_2,\lambda n} \end{pmatrix} \times \begin{pmatrix} \Delta c_{\mathrm{HbO}_2} \\ \Delta c_{\mathrm{HbR}} \end{pmatrix}. \tag{5}$$

While imaging absorption changes in superficial tissues appears quite straightforward, the effects of scatter must be carefully considered. Since scattering is wavelength dependent in tissues [an approximate scatter spectrum is shown in Fig. 1(a)], each measurement wavelength will experience different levels of scattering. The mean path of light through tissue (DPFx) will also be altered by the background absorption properties of the tissue, which are also heavily wavelength dependent, owing to the presence of hemoglobin, so $\mathrm{DPF}x_{\lambda 1} \neq \mathrm{DPF}x_{\lambda 2}$ in almost all cases. Therefore, as given by Eqs. (4) and (5), accurate estimates of these wavelength-dependent pathlength factors $\mathrm{DPF}x_{\lambda n}$ are required *even to calculate differential changes* in hemoglobin concentration ($\Delta c_{\mathrm{HbO}_2}$ and Δc_{HbR}).

Note, however, that if $I(t)/I(t_0)$ is measured at an isobestic point, and DPFx does not change over time, then $I(t)/I(t_0)$ will be directly proportional to $\Delta\mathrm{HbT}(t)$.

Estimation of this wavelength-dependent pathlength $\mathrm{DPF}x_\lambda$ is difficult. For exposed-cortex imaging, a Monte Carlo model of light propagation is generally employed.[35] Such a model requires estimates of the background absorption and oxygenation level of the brain tissue to predict the likely scattered paths of photons.[31] For camera imaging, the mean pathlength calculation should simulate a widely distributed illumination, and incorporate the numerical aperture of the camera's lens.

It has been demonstrated that incorrect estimates of $\mathrm{DPF}x_\lambda$ can directly impact the correct calculation of HbO_2, HbR, and HbT changes in tissue.[35] Note also that if only values of $\Delta\mathrm{HbO}_2(t)$ and $\Delta\mathrm{HbR}(t)$ are derived, that it is *not* possible to infer changes in absolute oxygen saturation $\Delta\mathrm{SO}_2 = \mathrm{HbO}_2(t)/[\mathrm{HbO}_2(t)+\mathrm{HbR}(t)] - \mathrm{HbO}_2(t_0)/[\mathrm{HbO}_2(t_0)+\mathrm{HbR}(t_0)]$ without first estimating the baseline absolute concentrations of HbO_2 and HbR.

Another important issue to be considered in 2-D imaging of the cortex is the depth sensitivity of the measurement. The detected light has scattered within the tissue, and reports absorption that it has experienced along its path. The majority of detected photons have predominantly sampled the very superficial layers of the cortex, whereas fewer have traveled deeply and managed to return to the surface. This means that the image of the cortex is a superficially weighted sum of signals from different layers. Since the cortex has a complex structure of large superficial vessels and deeper capillary beds, the relative contributions of these compartments to the overall signal can be difficult to interpret. Additionally, since the mean penetration depth of the light will also depend on its wavelength, all wavelengths have not necessarily interrogated exactly the same region of tissue, which can impact the quantitative accuracy of estimates of HbO_2, HbR, and HbT.

A typical hemodynamic response in the somatosensory cortex of a rat during a four-second forepaw stimulus (3 μs pulses at 3 Hz) is shown inset in Fig. 2. The hemodynamic response to stimulus is fairly slow, peaking several seconds after the first stimulus pulse. A large increase in HbO_2 is generally seen, along with an increase in HbT and a decrease in HbR. The overall timing characteristics of each hemoglobin type are different from each other, and contain information about the underlying oxygen delivery and consumption dynamics.[19,36,37] Some researchers routinely observe a short initial increase in HbR, attributed to rapid oxygen consumption at the site of neuronal activation.[29,31,33] The origin of this initial dip is somewhat contentious, and it is discussed further in Sec. 2.1.3. The data shown in Fig. 2 are an average response of 400 stimulus repetitions. It should be noted that individual stimulus responses are often affected by physiological noise, such as variations in baseline blood flow to the region and fluctuations in systemic parameters such as blood pressure.

Despite all of these important considerations, 2-D optical imaging of the exposed cortex has provided very significant and well validated observations of functional cortical hemodynamics. Specific examples of applications of these techniques are given at the end of this section.

Two-dimensional voltage sensitive dye imaging. As described before, intrinsic signal and hyperspectral imaging can report the hemodynamic response to functional activation in the brain. This hemodynamic response is generally assumed to spatially correlate with the underlying brain activity corresponding to neurons firing and conducting electrical signals. The interrelation between neuronal and hemodynamic activity is currently an area of intense research.[18,38,39] This neurovascular coupling is thought to be an essential part of normal brain activity and is believed to be disturbed by pathologies such as Alzheimer's disease and stroke.[40,41] Understanding whether it is possible to determine detailed information about neuronal activity *from* hemodynamic measures is also an important area of research, driven by the fact that clinical fMRI is currently only sensitive to hemodynamic changes.

Voltage sensitive dyes (VSDs) provide a way to optically detect neuronal activity in the *in-vivo* exposed-cortex. VSDs were first used in 1968[42] but received renewed attention in 1986 when they were demonstrated for *in-vivo* mammalian brain imaging by Grinvald and colleagues[43–45] studies that predate the first reported intrinsic signal measurements.[27] Since then, significant advances in digital detector technology, dye formulation, and staining strategies have led to established use of VSDs to visualize neuronal activity *in-vivo*[2,24,46,47] and also for mapping electrical activity in the heart.[48,49]

VSDs are molecules that generally bind across a neuron's membrane. Changes in membrane potential cause measurable changes in the fluorescence of the dye.[50] Since a large percentage of the total membrane area is dendritic, VSD signals reflect both spiking and synaptic activity.[42]

Calcium sensitive dyes (CaSDs) are compounds that increase their fluorescence in response to increases in calcium ion concentration. When cells such as neurons are loaded with CaSDs, it becomes possible to monitor intracellular calcium.[51] Since a calcium influx occurs when a neuron fires an action potential, the calcium dye's fluorescence can optically report this, providing a second tool with which to optically image neuronal activity.

To image these dyes, a similar system to that shown in Fig. 2 is used, with the filter wheel replaced by an excitation filter of the appropriate wavelength. A long-pass filter is placed in front of the camera to block excitation light and isolate the fluorescence emission. In some cases, a dichroic mirror is used such that the illumination light is reflected onto the brain, and emitted fluorescence passes through the dichroic to the camera (via a secondary emission filter to remove residual excitation light). This is the configuration of a commercially available VSD imaging system sold by Optical Imaging Incorporated (Rehovot, Israel).[2]

As shown in the inset of Fig. 2, the hemodynamic response to stimulus typically peaks 2 to 4 sec after the stimulus begins. The neuronal response is much faster. Measured using VSDs and CaSDs, neuronal responses typically peak within 25 to 100 msec, and are usually followed by an inhibitory or refractory period of negative signal, which returns to baseline at around 150 to 300 msec after the stimulus starts.[52] The black trace in Fig. 2 shows the fluorescence changes seen in the somatosensory cortex stained with Oregon Green 488 BAPTA-1, AM calcium sensitive dye (Invitrogen) during the 4-sec forepaw stimulus (3-μs pulses at 3 Hz). Very fast, individual responses for each stimulation pulse can be seen, in contrast to the very slow hemodynamic response. To capture these responses, a faster camera is required than for hyperspectral or intrinsic signal imaging (preferably <10 ms per frame).

Voltage sensitive dyes typically have quite low contrast (typical $\Delta F/F \sim 0.5\%$). As a result, they can be affected by changes in hemoglobin absorption due to heart rate, breathing, and of course functional activation. Two methods have been developed to overcome this. 1. New dyes have been developed that excite and emit at higher wavelengths, corresponding to regions where hemoglobin absorption is less significant [see Fig. 1(a)]. 2. Acquisition of data is often triggered on the heart beat and sometimes breathing of the animal.[2] Many repetitions are generally averaged, and "blank" acquisitions where no stimuli are presented are interleaved such that the final signal is given by the stimulated – blank data. Voltage sensitive dyes can only be used in animals at present, and are usually topically applied directly to the exposed cortex for 1 to 2 h before imaging commences.[53] Some VSDs have been shown to quickly photobleach or have phototoxic effects, and so illumination times are typically kept to a minimum. It is also important to note that the change in fluorescence or absorption of VSDs is usually a manifestation of a spectral shift in either the absorption or emission spectrum of the dye.[54] This means that measurement wavelength selection should not necessarily be based on the peak absorption and emission wavelengths, nor should broadband emission filters spanning the whole emission peak always be selected. The excitation and emission wavelengths should be selected based on areas of the spectrum where the largest *change* in intensity will result when a spectral shift occurs (e.g., a band on the falling side of the emission spectrum).[54] Note that selection of wavelengths may therefore determine whether an increase or de-

crease in absorption or fluorescence is observed in response to an increase in membrane potential.

CaSDs have much higher contrast than VSDs ($\Delta F/F \sim 5\%$) and hence, despite generally exciting and emitting in the visible spectrum, are not strongly affected by small hemodynamic changes (although the small dip after the calcium response in Fig. 2 may be due to the concurrent increase in HbT and HbO_2 absorption). The challenge with CaSDs is introducing them into the neurons successfully, which to date has required the addition of dimethyl sulfoxide (DMSO) and pluronic acid, followed by direct pressure injection via micropipette into the cortex and incubation of 1/2 to 1 h.[3,55] However, it is possible to achieve fairly uniform loading of neurons within an area of several millimeters of cortex, and to observe responses similar to those seen with voltage sensitive dyes. Unlike VSDs, CaSDs tend to increase the intensity of their fluorescence emission in the presence of calcium, without significant shifts in the spectral position of their emission and excitation bands.

Examples of the use of VSDs and CaSDs for neuroscience studies are given at the end of this section. Imaging of CaSDs with two-photon microscopy is described in Sec. 2.2

Laser speckle-flow imaging. Another recent development in 2-D optical imaging of the exposed cortex is laser speckle-flow imaging. While hyperspectral and intrinsic imaging provide measurements of the changes in HbO_2 and HbR concentrations, they do not explicitly measure changes in the flow rate of the blood. Flow is a very important parameter if the rate of oxygen delivery (and/or consumption) is to be calculated. Laser Doppler has been widely used to provide point measurements of blood flow in the brain. However, laser speckle-flow imaging of the exposed cortex can provide a spatially resolved image of the flow throughout the vascular network during functional activation.[56,57]

Acquiring laser speckle-flow imaging data uses a similar setup to that shown in Fig. 2. However, in this case, the light source is replaced with a divergent laser diode (typically at 780 nm). The camera then simply acquires rapid and high-resolution images of the exposed cortex, which appear to be low-contrast images of the speckle pattern from the laser illumination. The speckle pattern is caused by the coherent laser light scattering within the brain. If red blood cells are moving within the image, they cause the speckle pattern to vary over time. The rate at which the speckles change relates to how fast the red blood cells are moving. Laser Doppler measures this temporal modulation. However, within the camera image, this intensity fluctuation causes spatial blurring. By calculating the spatial uniformity of an area of camera pixels (e.g., 5×5 or 7×7), the amount of blurring can be quantified [from the pixel group's (standard deviation of intensity)/(mean intensity) for each time point]. This speckle contrast can be mathematically related to the correlation time, which gives a measure of the velocity of flow of the red blood cells.[56] Laser speckle-flow imaging has been performed simultaneously with hyperspectral imaging of the exposed cortex (by adding a second camera, a dichroic, and filters to block the laser light). This has enabled the cerebral metabolic rate of oxygen consumption to be calculated.[30,36,37] Examples of the use of speckle-flow imaging are given next.

2.1.3 *Imaging of exposed cortex: examples*

Exposed-cortex imaging has been applied to a wide range of research areas. We can broadly summarize these as: 1. functional imaging to investigate the sensory and cognitive processing functions of the brain, 2. functional imaging to improve understanding of the basic mechanisms of the hemodynamic and neuronal response to stimulus, and 3. study of the effects of diseases and treatments on the normal behavior of the brain. Next we describe a selection of recent studies applying exposed-cortex optical imaging techniques within these important brain imaging fields.

Functional imaging for sensory and cognitive processing research. Most regions of the brain's cortex appear to be dedicated to consistent tasks. Particularly in the sensory cortices, there is even spatial correspondence between, for example, the location of two whiskers on the snout of a rat and the two sites (or barrels) on the somatosensory cortex that respond when each whisker is flicked.[58,59] Different parts of the auditory cortex respond to different frequencies of sound.[60] Studies of these systems are prevalent throughout the functional imaging literature, but optical imaging of the exposed cortex is currently the only technique that can provide sufficient resolution to reveal the intricate nuances of these hemodynamic and neuronal responses.

Figure 3(a) shows a recent exposed-cortex optical imaging result revealing the spatially distributed cortical response to visual stimulus in anesthetized rat.[61] Cortical imaging data were acquired at 590 nm and the results reveal a very clear spatially correlated retinotopic map of the cortical responses to visual stimuli across the entire visual field of one eye. The purpose of this study was to determine whether it is feasible to use rats as a model to evaluate adaptation of visual cortical function in response to retinal degeneration, and for development of associated potential therapies.

Figure 3(b) shows an example of a highly complex study of the visual cortex of awake monkeys using both intrinsic signal (hemoglobin) and VSD imaging.[24] Three Macaca fascicularis monkeys had 'windows' surgically implanted into their skulls over their visual cortex (covering areas V1, V2, and V4). The cortical response to visual stimulus was then imaged repeatedly for up to 1 year using VSD RH-1691 (Optical Imaging Incorporated, Rehovot, Israel) to stain the cortex 1 to 3 times per week (excited at 630 nm±5 nm, emission: 650-nm long-pass). For studies of the visual cortex, it is very common to utilize two equivalent visual stimuli and display the difference between the two responses. This is because each response on its own consists of many different changes in the vasculature and tissue, so by subtracting two or more equivalent states, only the very specific difference between the stimuli responses should be revealed. In this case, Fig. 3(b) shows intrinsic signal ocular dominance maps (605-nm reflectance) generated by showing the monkey a pattern with either his left or right eye blocked (the baseline image of the exposed cortex is also shown). The difference between these two states therefore reveals the response of one eye as bright areas and the response of the other as dark stripes. The image shows that this part of the visual cortex processes similar areas of the image from each eye in close proximity to each other, interleaving them, rather than processing the full im-

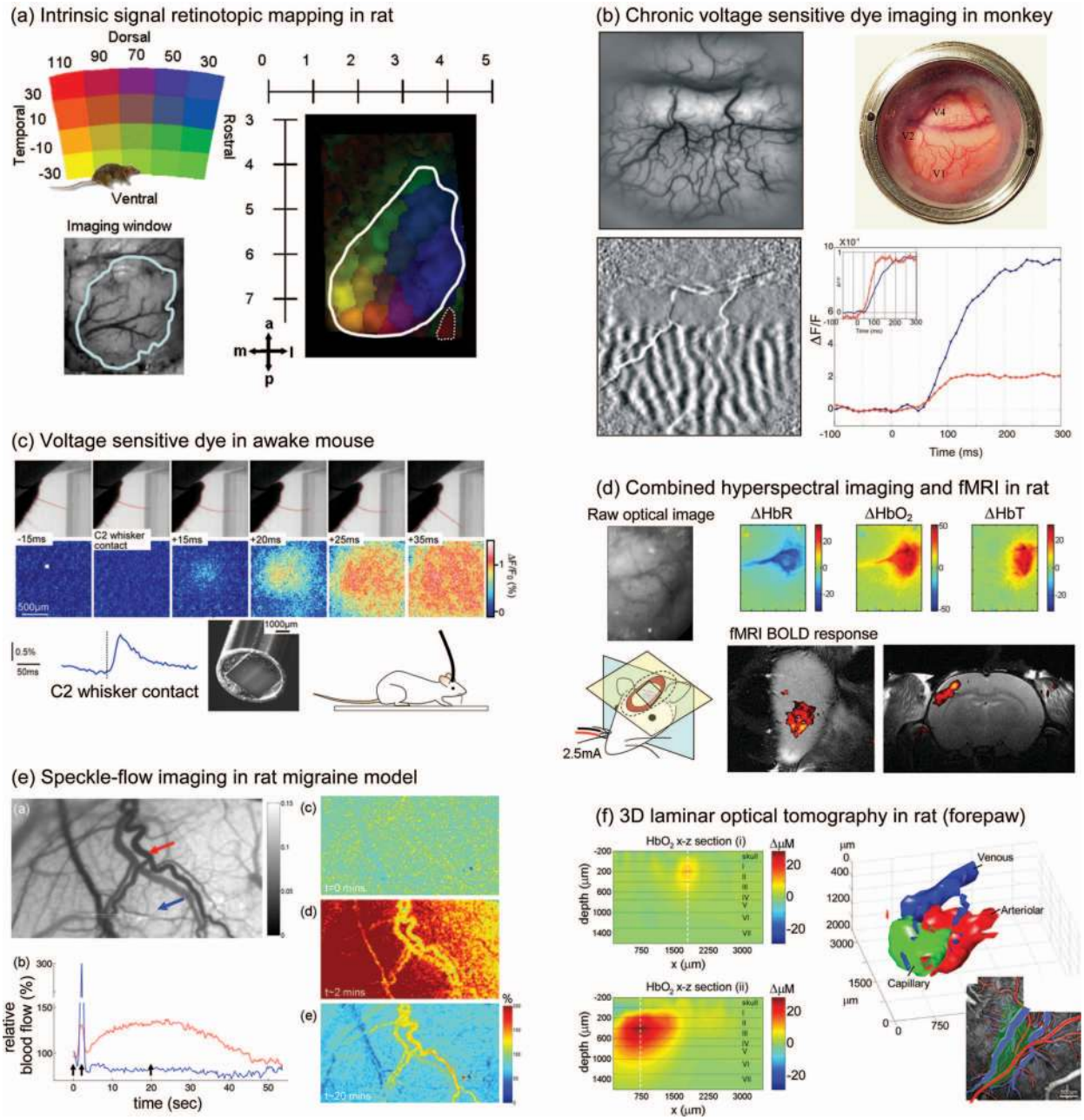

Fig. 3 Examples of *in-vivo* exposed cortex imaging. (a) Visual stimuli were presented in different parts of a rat's field of view, and the corresponding cortical hemodynamic HbT responses were mapped (color code indicates corresponding location of visual stimulus). Reproduced with permission from Gias et al.[61] (b) A cranial window was implanted to allow direct imaging of primate visual cortex. A baseline image of the exposed brain is shown above an intrinsic signal ocular dominance map, acquired by subtracting the response from visual stimulus to the right eye from the left eye. Chronic VSD imaging was also performed, and ocular dominance maps closely resembled intrinsic signals. Time courses of the voltage-sensitive signal (red) showed a more prompt onset that the hemodynamic response (blue). Reproduced with permission from Slovin et al.[24] (c) An optical fiber bundle was used to image the exposed, VSD stained cortex of an awake mouse while it explored its surroundings. Image series shows the mouse's whisker gradually brushing against an obstacle and the corresponding cortical response. Reproduced with permission from Férézou et al.[65] (d) A fiber optic bundle was used to image the exposed cortex of a rat undergoing electrical whisker stimulation during simultaneous acquisition of fMRI at 4.7 T. The hemodynamic response shows localized cortical changes in HbR, HbO_2, and HbT, which correspond well to oblique-slice fMRI BOLD response (study by Hillman, Devor, DeCrespigny and D'Arceuil). (e) Baseline speckle contrast image showing higher flow as darker contrast and strongly accentuated vessels. Image series from top to bottom show flow prior to induction of spreading depression, 2 min after which a wave of cortical flow increase moves across the field of view, and 20 min after, when hyperperfusion in the dural vessels is prominent. Plot shows time course of flow for region of interest in cortex (blue) and dural vessel (red). Reproduced with permission from Bolay et al.[15] (f) (left) Cross sectional *x-z* images through the cortical HbO_2 response to a 4-sec forepaw stimulus in rat imaged using laminar optical tomography, (top) transecting a superficial vein, and (bottom) transecting the deeper capillary response. (right) 3-D rendering of arterial, capillary, and venous compartment hemodynamic responses. *Ex-vivo* two-photon microscopy of vasculature (inset) agrees with compartment discrimination. Reproduced with permission from Hillman et al.[19]

ages from the left and right eyes separately. Very similar maps were seen for both VSD and intrinsic signal imaging, although the timing and evolutions of the neuronal and hemodynamic signals were quite different. The data shown here are just the introduction to a very broad study where similar maps were used to investigate the visual cortex's response to rapid saccadic eye movements. There are numerous other chronic optical imaging studies of monkey visual cortex[62] and monkey somatosensory cortex.[63] Very recent studies have also demonstrated that plasticity of ocular dominance can even be studied in mice using exposed-cortex optical imaging.[64]

Another recent novel approach to exposed-cortex optical imaging is shown in Fig. 3(c). While most rodent measurements use anesthetized animals, some studies of native behavior require that the animal be both awake and able to freely move around. Férézou, Bolea, and Petersen developed a technique where a mouse's voltage sensitive dye-stained exposed somatosensory cortex could be imaged via a flexible fiber bundle while the awake mouse explored its surroundings.[65] By simultaneously acquiring video of the mouse's behavior, they were able to directly image the neuronal response in the brain when the mouse's whisker contacted an object.

Functional imaging to investigate the mechanisms of activation. The functional imaging studies described above exploit the fact that colocalized neuronal and hemodynamic responses can be detected in the brain in response to stimuli.[26] However, very little is understood about how and why these functional responses actually occur.[40,41,66] Understanding the origins and characteristics of these responses, and the interplay between neuronal and hemodynamic processes, is key to developing an improved picture of healthy and impaired brain function. It is also an essential part of developing and improving all functional brain imaging modalities that rely on the contrast provided by hemodynamic changes such as fMRI. Since exposed cortex optical imaging can provide such a close view of the working brain, as well as access for invasive measurements such as electrophysiology, it has become an established tool for the study of basic functional mechanisms.

A wealth of recent studies have investigated so-called neurovascular coupling (NVC) relationships using optical methods.[18,31,38,39,58,67–69] By quantifying the hemodynamic response (via optical imaging and/or laser Doppler) simultaneously with the neuronal response (via electrophysiology), these studies sought to identify a parametric relationship that could be used to predict one response from the other. Devor et al. demonstrated in rat that within a single whisker barrel, the neuronal response to different amplitudes of tactile whisker stimulus saturated before the hemodynamic response.[18] More recently, subtleties of the spatiotemporal evolution of both responses have shown that the NVC relationship is highly complex.[58,70] A recent study also demonstrated that there can be significant differences between the responses of anesthetized and awake rodents.[23]

An alternative to attempting to infer neuronal responses from BOLD-type measurements is to instead locate sites where oxygen consumption is increasing by determining the cerebral metabolic rate of oxygen consumption ($CMRO_2$).[71,72] In principle, these regions should spatially correlate more closely with neuronal activity than the BOLD response, which can be significant even in distant draining veins.[73] $CMRO_2$ is a parameter that can only be calculated by considering the amount of oxygen that is delivered to and extracted by the tissue. Although 2-D hyperspectral imaging can provide changes in HbO_2, HbR, and HbT concentration, the data represent discrete snapshots of the current oxygenation state of the blood, and not the rate at which the blood is being replaced. It is therefore necessary to also measure blood flow, to determine the rate of delivery of oxygen to the tissue. Other estimates are also required such as the variations originating in the venous compartment. Both laser Doppler and more recently speckle-flow imaging have allowed simultaneous measurement of oxygenation, blood volume, and flow dynamics in the exposed cortex,[30,36,37] thereby allowing direct calculation of $CMRO_2$. These calculations are based on models of the hemodynamic response to stimulus.[32,74–78] Interestingly, *in-vivo* optical imaging and microscopy of the cortex are also allowing the vascular mechanisms of the hemodynamic response underlying these vascular models to be investigated directly.[19,79,80]

Another approach to comparing exposed-cortex optical imaging findings to fMRI is to perform fMRI studies and optical measurements on the same subjects in response to the same stimulus. Several recent studies have demonstrated simultaneous optical imaging of the exposed cortex during fMRI acquisition.[81] An example of such a study is shown in Fig. 3(d), where an MRI-compatible fiber optic endoscope was configured to allow synchronized fMRI and functional optical imaging at two wavelengths (570 and 610 nm) during electrical whisker stimulus of varying amplitudes.

Similar studies have been performed in humans scheduled to undergo open cortex brain surgery[21,82,83]: functional responses to voluntary motion of the tongue were recorded in the language area of the brain prior to surgery using fMRI, and then compared to optical imaging results obtained during surgery, where the awake patient was asked to repeat the same stimulus paradigm.[83] These results were compared to electrocortical stimulation maps acquired by directly stimulating the cortex and questioning the patient about the resulting involuntary tongue movements.

A final optical imaging result of significant importance, and which has prompted much debate, was the discovery of the so-called "initial dip."[33] In some studies, the hemodynamic response to stimulus is seen to begin with an increase in HbR, prior to a subsequent decrease. This finding was interpreted as evidence that neurons initially use up local oxygen more quickly than it is being supplied by the gradually increasing blood flow, an important finding for modeling the mechanisms of the hemodynamic response. It was proposed that this early signal could also allow improved spatial localization to the neuronal response. This initial HbR rise was subsequently also seen in fMRI results as an initial dip in the BOLD signal,[84,85] and in many other optical imaging studies.[29,37,86] However, the dip is controversial because it is not seen in all studies.[87] Reasons proposed for this discrepancy have ranged from differences between species, anesthesia, and paradigms, to measurement techniques and errors in spectroscopic analysis of optical signals (especially the wavelength dependence of pathlength[88]). An excellent summary of the initial dip can be found in Ref. 89.

Functional imaging to investigate pathologies and treatments. A further use of exposed cortex imaging is to directly investigate the manifestation, characteristics, and treatment responses of diseases and disorders. An example of one such study is shown in Fig. 3(e), which used speckle-flow imaging to investigate migraine in a mouse model.[15] Cortical spreading depression (CSD) is a slow moving wave of neuronal and hemodynamic activity that spreads across the cortex following a small insult to the cortex, such as a pin prick.[90] CSD is thought to be the cause of the visual disturbances that often precede a migraine headache. This study demonstrated that speckle-flow imaging could not only see the wave of CSD as a transient increase in parenchymal blood flow, but also revealed a prominent subsequent increase in blood flow in the middle meningeal artery (MMA), a vessel that traverses the dura. Such a dural blood flow increase is consistent with the delayed onset of a debilitating migraine headache. Supporting measurements were then made to conclude that CSDs can trigger events leading to headache, identifying new pathways that could potentially be targeted for the development of treatments for migraine suppression.

Similar studies using both speckle flow imaging and hypersepctral imaging of the exposed cortex have examined the effects of middle cerebral artery occlusion as a model of stroke.[13,91] Both the acute stage and chronic manifestations of stroke can be studied. Function of the area affected by a stroke can be evaluated after days or even weeks of recovery.[92,93] The effects of established and experimental treatments can be tested in these models of human stroke, and even compared to the fMRI manifestation of the same outcomes.[94]

It is also possible to study epilepsy in animal models using exposed-cortex intrinsic signal optical imaging[95] and VSDs.[96] The hemodynamic response to intrasurgical cortical stimulation during epilepsy surgeries on humans has also been investigated using optical imaging.[22]

2.1.4 *Methodological extras*

In addition to the three basic 2-D imaging techniques described before, a number of other distinct optical exposed cortex imaging approaches have recently been demonstrated and are described briefly next.

Intrinsic fluorophore imaging. Several recent studies have shown compelling evidence that it is possible to measure concentration changes in intrinsic flavoproteins (FAD) in the brain from their intrinsic fluorescence *in vivo*.[97–100] A system almost identical to that used for VSD imaging is employed, but no contrast agent is added to the brain. Excitation is between 450 and 490 nm and emission is between 500 and 550 nm. FAD provides a measure of metabolic changes in cells (neurons and possibly glia), and has a distinct time course compared to shorter neuronal and longer hemodynamic responses. FAD imaging was recently used to explore visual plasticity in mice in a similar way to the studies of the visual cortex described before,[101] as well as plasticity in the auditory cortex[102] and epileptic activity.[103] Since flavoprotein fluorescence requires visible light for its detection, it is unlikely that it will be possible to detect these signals noninvasively (see Fig. 1).

Fast scattering signal. Another source of intrinsic optical signal in the brain is the fast scattering signal. Historically, this signal has been the source of much debate, particularly related to the difficulties in detecting it noninvasively,[104,105] although the signal is clearly observable in isolated nerves.[106] Recently, exposed cortex measurements during whisker stimulation in rats have provided compelling data revealing localized signals corresponding to regions of neuronal activity.[107] Changes in the dark-field reflectance of 660-nm light occurred within 50 ms of stimulation and correspond well with electrophysiological recordings. A 4-mm-diam imaging probe was placed in direct contact with the dura over the exposed somatosensory cortex. The probe consisted of an outer ring of optical fibers delivering illumination light from 660-nm light emitting diodes, and a central fiber optic imaging conduit transmitting remitted light to a sensitive charge-coupled device (CCD) camera. Several possible mechanisms for the origin of the fast scattering signal have been proposed, including reorientation of membrane proteins and swelling of neuronal dendrites due to water influx in response to ionic currents during depolarization.[107]

Note that the possibility that fast scattering changes in the brain may distort and interfere with VSD intensity signals has not yet been explored. It is also still not fully understood whether significant scattering changes occur in the brain as part of the (slower) hemodynamic response. Some researchers have tried to compensate for scattering changes by including a scattering spectrum term in Eq. (2), as if it represents a third chromophore.[33] Care should be taken with this approach, since it does not completely account for scattering effects, and incorporating a third chromophore (which may not in fact be changing) may adversely affect the fit results of the other two chromophores (HbO_2 and HbR).

Optical coherence tomography of functional brain activation. Optical coherence tomography (OCT) is a well established technique for high resolution depth-resolved imaging of structures such as the eye.[108] OCT overcomes the effects of light scattering to obtain high resolution depth-resolved images by using coherence to isolate light that has been directly backscattered. This light therefore has the shortest possible pathlength through the tissue. OCT is also typically performed using NIR wavelengths >1 μm. As a result, OCT signals carry very little information about the hemoglobin absorption properties of tissue [Eq. (1) and Fig. 1] and cannot be used to measure fluorescence contrast. The contrast in OCT is therefore generally due to refractive index mismatches, and not due to changes in absorption corresponding to hemoglobin concentration or oxygenation. Nevertheless, OCT has recently been applied to brain imaging to explore depth-resolved changes in the cortex of cats and rats during functional stimulus.[109–111]

To date, the functional OCT changes reported have followed the slower time scale of the hemodynamic response. Both increases and decreases in OCT contrast are seen in close proximity, at times when HbT should be increasing. It is possible that OCT could also detect fast neuronal scattering signals. However, the slower signals observed to date are hypothesized to correspond to changes in the speed and distribution of scattering red blood cells, and changes in diameter and tone of pial vessels and capillaries.

Laminar optical tomography. While 2-D optical imaging of the exposed cortex has found many very valuable applications, there remains concern over the fact that images are a 2-D projection of a combination of signals from superficial vessels and deeper layers of the cortex. The vascular structure of the cortex is organized with large arteries and veins on the surface, and then arteriolar and venous branches diving almost straight down to deeper capillary beds. These capillary beds supply the active neurons, which themselves are also organized in specific layers within the cortex. Therefore, not only are neuronal and vascular signals likely to be quite heterogeneous as a function of depth, but the laminar variations in neuronal and hemodynamic responses are of great interest. Laminar optical tomography (LOT) is a recently developed imaging technique that can add a depth dimension to hyperspectral imaging of the exposed cortex.[19,112,113]

LOT utilizes a combination of scanning microscopy instrumentation and optical tomographic image reconstruction techniques to acquire noncontact measurements of the cortex at more than 40 frames per second. It can image to depths of >2 mm with 100 to 200-μm resolution. A recent result is shown in Fig. 3(f), where LOT was used to image the exposed-cortex hemodynamic response to rat forepaw stimulus at 473 and 532 nm. The depth-resolved images were validated by comparison to the vascular architecture, and microsvascular density determined via two-photon imaging of fluorescent vascular casts from the same animals. A spatiotemporal delineation technique was also applied that exploited the distinct differences in the temporal evolution of the functional signal in the different vascular compartments: arterioles, capillaries, and veins. Figure 3(f) shows two cross sectional $(x-z)$ images through the HbO_2 cortical response, one transecting a superficial vein, and one transecting the deeper capillary response. A 3-D rendering of the three vascular compartments, delineated via their distinctive time courses, is also shown, revealing superficial arterioles and venules, and deeper capillary responses. A two-photon image of a vascular cast from the same animal is shown alongside, with the corresponding arterioles and veins highlighted. The temporal signatures of each different vascular compartment were cross-validated with *in-vivo* two-photon imaging and provided new insights into some of the basic assumptions of the hemodynamic models for fMRI interpretation described before.[19]

Since LOT detects scattered light, it is highly sensitive to blood oxygenation and HbT changes and is also suitable for fluorescence imaging. As a result, LOT in now being developed to allow simultaneous depth-resolved imaging of hemodynamics and VSDs or CaSDs. Depth-resolved imaging of VSDs and CaSDs would allow the laminar properties of neuronal responses to be studied in detail. Currently, such measurements can only be made using highly invasive depth-resolved electrode arrays, although demonstration of a gradient index lens-based system also recently showed promising results imaging VSDs in mouse cortex to depths of 150 μm.[114]

2.2 *Two-Photon Microscopy*

Two-photon microscopy is a distinctly different functional imaging technique compared to the optical imaging described so far. Two-photon microscopy was first demonstrated in 1990,[115] and has since become an invaluable tool for imaging intact biological specimens at very high resolution, to depths of up to 600 μm. Two-photon microscopy has more recently been applied to *in-vivo* imaging of the brain.[3,19,79,116,117] While fluorescent contrast is required, two-photon microscopy provides an unprecedented view of *in-vivo* brain activity on a cellular and microvascular level.

2.2.1 *Two-photon microscopy: basic principles*

Two-photon microscopy is similar to confocal microscopy, in that it requires a focused beam of laser light to be steered within tissue, sensing the properties of each location and using them to form a 2-D or 3-D image. Confocal microscopy relies on the rejection of scattered light by isolating signals originating from the focus of the scanning beam. Confocal xcitation wavelengths are typically in the visible spectrum, where tissue scatter and absorption are high (see Fig. 1). Therefore, when using confocal microscopy to image to depths beyond 200 to 300 μm, the laser beam can no longer focus, and images become blurred and lack sensitivity. Also, while it is assumed that the detected fluorescent light originates from the focus of the scanning beam, some of the detected signal is also generated by excitation and emission light that is scattered or absorbed within the tissue above and below the focus. Not only does this light contribute to image blurring, it can also result in cumulative photodamage to areas of the tissue that are not actively being imaged.

Two-photon microscopy overcomes many of the disadvantages of confocal microscopy. Instead of exciting fluorophores at visible excitation wavelengths, two-photon microscopy utilizes laser light of twice the excitation wavelength. When sufficient photon flux is achieved, it is usually possible for a fluorophore to be excited by two of these lower energy photons arriving in quick succession. Once excited, the fluorophore will emit a photon at (or near) its usual emission wavelength. This is illustrated schematically in Fig. 4(a). This high photon flux is achievable if a pulsed laser is used, which delivers very high energy, rapid pulses (typically a Ti:sapphire laser, tunable between $\sim$700 and 1000 nm, with 80-MHz pulse repetition, $<$500-fs pulse width, mean power 1 W, peak power 25 kW). Even with such high peak power, the nonlinear effect of two-photon excitation will only happen at the tight focus of the laser beam. As a result, two-photon microscopy can use NIR light to image the same fluorophores as confocal microscopy. However, since scattering and absorption of NIR light in tissue is much lower than for visible light [see Fig. 1(b)], the laser beam's focus can be maintained to depths of $>$600 μm, depending on the tissue type. The fact that fluorophore excitation only occurs at the very focus of the beam means that surrounding tissue does not experience significant photodamage. The NIR excitation light is generally spectrally well separated from the emission wavelength, making rejection of excitation light much simpler than for confocal microscopy. Further, since it is expected that any light emerging from the tissue at the fluorescent emission wavelength at a particular time can *only* have originated from the focus of the scanning beam, it is not necessary to attempt to reject scattered light, as required in confocal microscopy. Instead, sensitive detectors can be placed as close to the tissue as possible to collect all of the emerging emission light. This

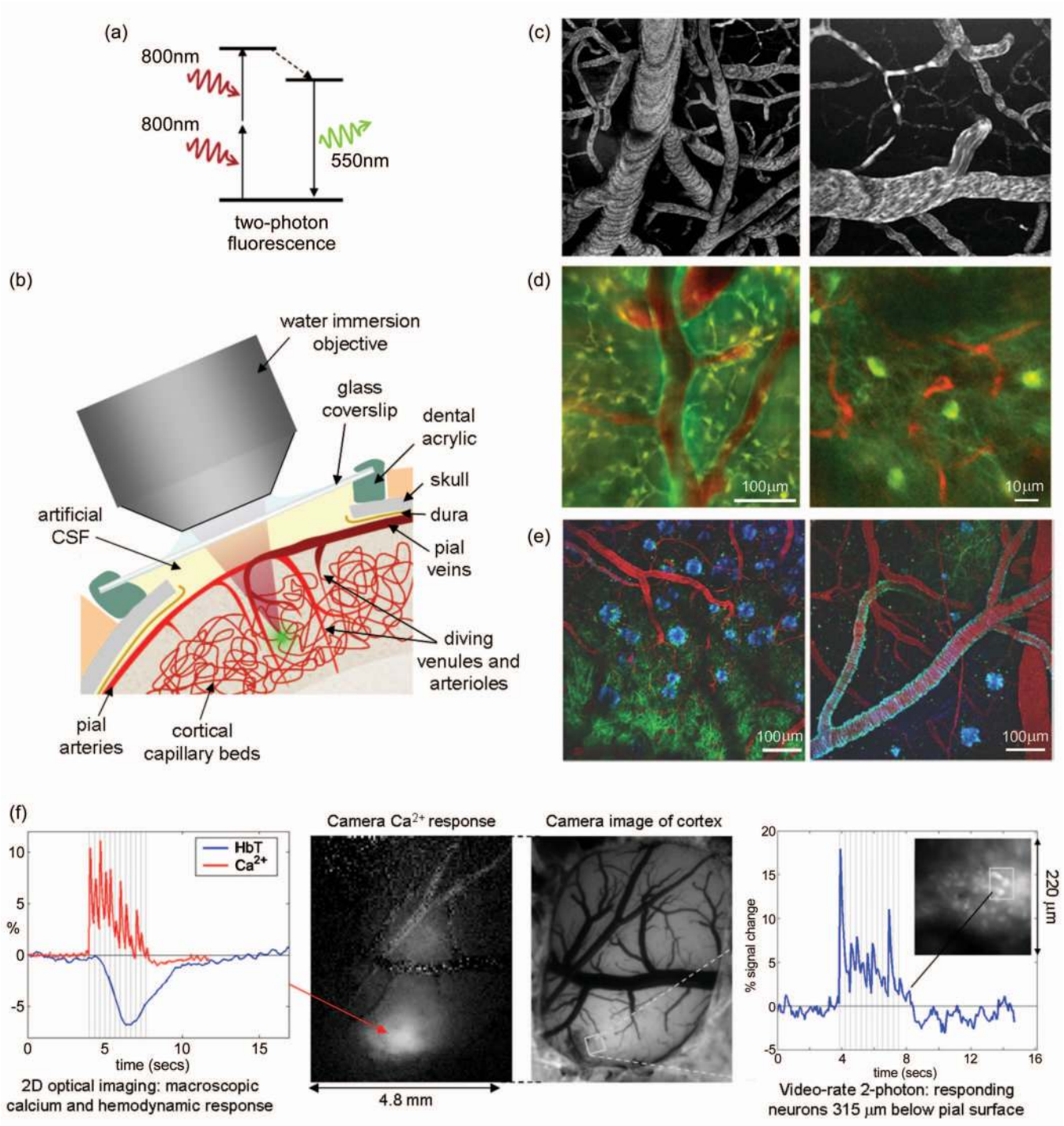

Fig. 4 Two-photon microscopy of *in-vivo* brain function. (a) Basic mechanism of two-photon fluorescence. (b) Schematic of surgical preparation of exposed cortex, with sealed glass window and microscope objective positioning. Green dot shows location of two-photon fluorescence. (c) Examples of two-photon maps of the vasculature following intravenous injection of dextran-conjugated fluorescein. Black dots and stripes show red blood cell motion. (d) Dual-channel imaging of neuronal (green) and vascular (red) signals: (left) Oregon Green 488 BAPTA-1 AM calcium-sensitive dye stained neurons and (right) transgenic mouse expressing green fluorescent protein (GFP) in a subpopulation of neurons (mouse supplied by Friedman, Rockefeller University, New York[130]). Texas dextran red is the intravascular tracer in both cases (studies by Hillman, Bouchard, Ruvinskaya and Boas). (e) Three-channel imaging of Tg2576 APP Alzheimer's disease mouse model with amyloid-β targeting dye (blue), GFP expressing neurons and dendrites (green), and vasculature (red). Reproduced with permission from Spires et al.[14] (f) 2-D camera-based imaging of hemodynamics and calcium response followed by functional two-photon imaging of the calcium response on the scale of single neurons in the same rat. Oregon Green 488 BAPTA-1 AM was loaded with serial pressure injections into the cortex. Stimulus was ~1 mA, 3-μs pulses at 3 Hz for 4 sec (studies by Hillman, Bouchard, Ruvinskaya and Boas).

Table 1 Summary of optimal two-photon microscope characteristics for *in-vivo* brain imaging.

Feature	Custom-built *in-vivo* two-photon microscopy systems	Commercial two-photon microscopy systems
Form factor	Almost always upright.	Often inverted.
Imaging platform	Fixed *Z* stage (objective moves up and down, not stage). Motorized $x-y$ stage. Very open clearance around objective for animal and monitoring equipment.	Require *Z* translation of stage, poor clearance between stage and objective. Motorized $x-y$ stage movement very expensive.
Detection geometry	Detectors positioned very close to back of objective for maximum light collection. Multiple spectrally resolved detectors may be stacked to allow two or more emission wavelengths to be simultaneously imaged.	Two-photon detector may be in place of confocal detector, therefore descanned and through pinhole—very poor light efficiency. Otherwise retrofitted detectors are rarely close to the objective.
Numerical aperture	Very high numerical aperture (but long working distance) allows good *z* resolution, high efficiency, and ability to image through exposed-cortex preparation [see Fig. 4(b)].	Similar objectives can be chosen for commercial systems if compatible.
Scan rate	Typically designed to allow very high frame or line-scan rates to image dynamics of functional activity.	Frame rate well optimized, but limited adaptability for patterns and line scans.
Software	Custom software allows wide variety of scan patterns and routines for a wide range of experiments.	Often proprietary and difficult to modify. Fixed scan patterns and routines.
Multimodality	Typically possible to add additional imaging and measurement modalities to the system owing to accessible light path and animal. Can be integrated into custom software.	Very difficult to modify or interrupt light path.

signal, when reformed according to the beam scanning pattern, produces a high resolution image of the fluorescent structures within tissue. Where traditional microscopy required tissues to be stained and sectioned, two-photon microscopy therefore allows high-resolution 3-D imaging of intact, functioning tissue.[118]

Techniques have been developed to allow *in-vivo* imaging of the exposed cortex of animals, and the use of two-photon microscopy for neuroscience research is now widespread.[119] After exposing the cortex as described in Sec. 2.1.1, a typical approach is to then apply or inject topical dyes and subsequently cover the exposed brain with agarose in artificial cerebrospinal fluid (CSF).[120] A small glass cover slip placed over the opening in the skull and sealed in place using acrylic cement can be used to effectively reseal the skull, allowing intracranial pressure to re-equalize, preventing contamination or dissolution of ambient gases and controlling brain movement (which would otherwise be substantially affected by heart rate and breathing). Measurements would typically proceed while the animal continued to be anesthetized, although some researchers have implanted sterile windows or artificial duras that can stay in place for up to a year, allowing longitudinal studies.[14,24,121]

Apart from access to the brain, two difficulties with implementing two-photon brain imaging remain. First, the cost of the laser required for imaging is currently high ($100,000 to $200,000 USD). The second difficulty is that, while commercial two-photon microscopy systems exist, to date most are based on modified confocal microscopy systems, and are also very expensive. This means that some of the benefits of two-photon microscopy are not fully exploited, and modification of the systems to allow live animal imaging is difficult or impossible. As a result, many researchers have instead built their own two-photon microscopy systems, optimized for *in-vivo* imaging.[122–126] Table 1 summarizes the key attributes of *in-vivo* two-photon microscopy systems that are specifically designed for *in-vivo* imaging.

2.2.2 *Two-photon microscopy: examples*

As for 2-D optical imaging, *in-vivo* brain imaging research using two-photon microscopy has also found applications in areas of functional processing, functional mechanisms, and disease research. These applications utilize a variety of methods to introduce fluorescent contrast to the brain, including intravenous injection of dextran-conjugated dyes to reveal blood vessels, topical application, or pressure injection of dyes into the cortex, systemic delivery of dyes that cross the blood brain barrier, and transgenic mutation of cells to express fluorescent proteins. Examples are given below.

Functional processing. A recent example of *in-vivo* two-photon microscopy of brain function was the use of calcium-sensitive dyes to look at visual responses in cats and rats.[3,127] Data were acquired using a custom-built two-photon microscope, and used Oregon Green 488 BAPTA-1 AM dye (Invitrogen) excited at 800 nm to provide calcium-sensitive fluorescent contrast. The dye was pressure injected into the cortex as described before for 2-D imaging of CaSDs. The complex cortical patterns of the response to visual stimuli of different orientations [similar to the ocular dominance maps in Fig. 3(b)] were found to occur even on the scale of discrete individual neurons.

Functional mechanisms. The advent of functional two-photon microscopy has allowed the mechanisms of neurovascular coupling to be studied *in vivo* in unprecedented detail. Whereas 2-D optical imaging of the cortex, as described earlier, has enabled parametric comparisons between electrophysiology and the hemodynamic response,[18] two-photon imaging enables the interrelations between individual neurons, glial cells, and vessels to be examined in intricate detail.

Both confocal microscopy[128] and two-photon microscopy[79] have been used to examine the dynamics of red blood cells flowing through capillaries in the exposed cortex. In Ref. 79 and more recently in Refs. 116 and 129, the capillary response to stimulation and hypercapnia have been examined using fluorescent plasma tracers such as dextran conjugated fluorescein or Texas dextran red (Invitrogen). These high molecular weight dyes cannot pass the blood brain barrier or stain red blood cells, and so provide strong contrast to vessels. Typical *in-vivo* image stacks of fluorescein-perfused vessels in rat brain are shown in Fig. 4(c). The dark stripes and dots are moving red blood cells whose dynamics can be quantified from their motion in sequential images or line scans.[126] The flow and dilation dynamics of pial arterioles and veins was also recently investigated using two-photon microscopy.[19]

Figure 4(d) (left) shows simultaneously acquired *in-vivo* rat brain measurements of neurons labeled with Oregon Green 488 BAPTA-1 AM dye and vessels containing Texas dextran red. Both color channels were acquired with two-photon excitation at 800 nm and 550-long-pass dichroic and emission filters to separate the two emission bands onto different photomultiplier detectors. Figure 4(d) (right) shows similar data acquired in a transgenic mouse, engineered such that only certain neurons in the brain express green fluorescent protein.[130,131] Capillaries perfused with Texas dextran red can be seen to be weaving amidst the webs of dendrites.

2-D optical imaging of hemodynamic and CaSD changes can also be acquired prior to imaging the same animal with two-photon microscopy. Figure 4(f) illustrates 2-D imaging of the calcium-sensitive Oregon Green 488 BAPTA-1 AM response in the somatosensory cortex of a rat during forepaw stimulus (1.5 mA, 3-μs pulses at 3 Hz for 4 sec), followed by two-photon imaging of individual neurons at a depth of 315 nm in the cortex responding to the same forepaw stimulus. The two-photon fluorescence of the CaSDs increased by up to 17% during stimulation.[126]

Such direct and simultaneous observations of both neuronal and hemodynamic responses and structures in *in-vivo* systems enable the intricate mechanisms underlying neurovascular coupling relations to be closely examined and compared to macroscopic-scale measurements and even fMRI results.

Two recent studies used similar two-photon imaging techniques to present compelling evidence supporting the role of astrocytes as active mediators of blood flow control.[80,132] Astrocytes make up a large fraction of the cells in the brain, and have been shown to be both metabolically active and capable of transmitting signals between neurons and blood vessels.[133,134] In Ref. 132, astrocytes in mouse brain were labeled with calcium-sensitive rhod-2 AM, caged Ca^{2+}, and DMNP-EDTA AM, while the vasculature was perfused with dextran conjugated fluorescein. Two-photon imaging of astrocytic endfeet contacting arteries was performed *in vivo* at 825 nm, with spectrally separated detectors for rhod-2 AM and fluorescein. A second laser (355 nm) was then focused onto an endfoot and pulsed to cause photolysis of the DMNP-EDTA, triggering intracellular uncaging of calcium in the endfeet. This forced increase in calcium caused the endfoot to dilate. In a subsequent study, a CaSD (fluo-4 AM) and astrocyte-specific dye SR101 were used to demonstrate that similar calcium increases in astrocytic endfeet could be observed during prolonged whisker stimulation *in vivo*.[80]

Functional imaging to investigate pathologies and treatments. In-vivo two-photon imaging of intravascular dextran-conjugated fluorescein in rats was recently used to investigate the effects of stroke on blood flow dynamics, as well as the recovery of flow following two treatments: hemodilution and injection of a recombinant tissue-type plasminogen activator.[135] The study also *created* the strokes using a second laser delivering targeted high fluence ultra-short NIR pulses to cause vessel rupture, intravascular clotting, or extravasation of blood components depending on the laser power.

Alzheimer's disease research has been greatly impacted by the availability of fluorescent markers that bind to beta amyloid plaques in the brain.[5,136,137] The so-called Pittsburg compound B [2-(4'-methylaminophenyl)-6-hydroxybenzothiazole, PIB] can be used as a clinical contrast agent for PET imaging and is showing promise as a diagnostic tool in humans.[138] However, since PIB is fluorescent, it can also be used as a two-photon microscopy contrast agent for exposed cortex imaging.[117] Tg2576 APP transgenic mice develop beta amyloid plaques over the course of their lives, and are assumed to provide a realistic model of the progression of Alzheimer's disease. Since Alzheimer's in humans can currently only be confirmed postmortem, these mouse models offer an opportunity to investigate the early effects of the disease, as well as learn about its progression and to allow development of earlier treatment and diagnostic methodologies.

Mice with chronically implanted cranial windows can be repeatedly imaged with two-photon microscopy for up to a year. This has allowed two-photon microscopy to be used to evaluate the effect of developing amyloid-β plaques on the structure and function of surrounding neurons and blood vessels. Figure 4(e) shows three-channel two-photon image stacks of the brain of a 21 to 24 month old transgenic mouse with beta amyloid deposits shown in blue, blood vessels (perfused with Texas dextran red) shown in red, and neurons expressing green fluorescent protein in green. The amyloid binding dye (methoxy-XO4, similar to PIB) was injected intraperitoneally the day before imaging. The neurons were labeled by transfection from an adeno-associated virus injected into the brain 2 to 3 weeks prior to imaging.[14] Extensions of this work to noninvasive animal and perhaps even human imaging are being explored.[139]

2.2.3 *Methodological extras*

Fluorescence lifetime imaging and microscopy (FLIM) has also been applied to neuroimaging, allowing potential enhancement of intrinsic contrast via environment-dependent lifetime shifts. FLIM has also been utilized to improve measurements of fluorescence resonance energy transfer (FRET),

which can provide measures of the proximity of two fluorescently labeled entities and therefore direct visualization of biochemical interactions.[140]

There is an extensive body of neuroscience literature that utilizes living brain slices to study neuronal activity in intricate detail. Mice and rats are rapidly sacrificed before their brains are removed, sliced, and placed in a carefully prepared perfusate that supplies nutrients and oxygen. Important results have been obtained by imaging brain slices with two-photon microscopy. For example, using brain slices, Kasischke et al. demonstrated that it was possible to use two-photon microscopy to measure the intrinsic fluorescence of NADH, and distinguish between cytoplasmic and mitochondrial NADH dynamics.[141] It has also recently been shown that voltage-sensitive responses in neurons and dendrites in brain slices can be measured via second harmonic generation (SHG) microscopy when neurons are loaded with a SHG contrast enhancing agent called FM4-64.[142,143]

3 Noninvasive Optical Brain Imaging

For routine optical brain imaging in humans, it is clearly necessary to develop noninvasive techniques. Approaches must overcome the effects of light scattering, while maintaining the strong benefits of functional optical contrast. To date, noninvasive optical brain imaging has been applied to babies, children, and adults for studies of functional activation, and for investigation of pathologies.

Since light penetration and scattering are significant obstacles for noninvasive imaging, measurements on children and babies are easier to achieve. It is often difficult to image these infants and small children using fMRI and PET, and so optical imaging provides a unique opportunity to study many aspects of functional brain development that have previously been inaccessible.[144] Imaging of pathologies in infants is also highly motivated by the prevalence of perinatal brain injuries due to prematurity, birth asphyxia, and congenital conditions.[34] Thanks to the portable and nonionizing nature of optical imaging, it is possible to obtain optical measurements on babies within a neonatal intensive care unit,[145] and on young children who are able to sit on a parent's lap in a familiar environment.[146]

Optical imaging of the adult brain can also provide valuable functional information that complements modalities such as fMRI. A particular advantage is optical imaging's ability to simultaneously image HbO_2, HbR, and HbT. Optical imaging is being widely adopted for studies of the cortical hemodynamic response to a wide range of stimuli.[147–158] Multimodality imaging of the adult head *during* fMRI,[150,159,160] electroencephalography (EEG)[161] and magentoencephalography (MEG)[162] has provided insights into the contrast mechanisms of the fMRI BOLD signal, and allowed oxygen consumption and neurovascular coupling relations to be investigated in humans. Optical imaging in adults is also being used as a tool for monitoring and detecting hematomas and stroke, as well as the effects of other pathologies and surgery on brain perfusion.[147,163–165] Noninvasive optical imaging holds the potential to provide accessible monitoring of brain function in situations where other imaging modalities such as fMRI are prohibitive, e.g., due to imaging environment or cost.

Noninvasive optical brain imaging on animals is generally performed as a precursor to clinical imaging in babies and adults. It may also be used to improve understanding of clinical data, including studies of neurovascular coupling, stroke, birth asphyxia, etc.[166–169] Noninvasive animal optical brain imaging has also been used for longitudinal development studies,[170] and measurements where exposing the cortex is not feasible, or would detrimentally affect the experiment.

There are two main technological approaches to noninvasive optical brain imaging: fairly simple topographic measurements of cortical function [as shown in Figs. 5(a) and 5(b)], and 3-D tomographic imaging of the brains of infants [as shown in Figs. 5(c) and 5(d)]. The basic principles of these approaches are described next, followed by specific examples of their *in-vivo* neuroimaging applications.

3.1 *Topography*

3.1.1 *Experimental method*

Noninvasive topographic optical measurements of the human head can interrogate hemodynamic changes in the cortical surface of the brain [Fig. 1(b)]. The majority of functional processing occurs in the cortex, and so optical topography is commonly, and extensively, used to measure functional responses to stimulus in children and adults.

Early classifications of the roles of the different areas of the cortex were deduced from observations of the effects of injuries to different parts of the brain.[171,172] More recently, these cortical areas have been refined and investigated using functional brain imaging modalities, including fMRI and animal imaging studies such as those described in Sec. 2. Figure 5(e) shows the basic regions of the cortex and their functional roles. Optical imaging studies of brain function often focus on the occipital or visual cortex at the back of the head (looking at responses to visual stimulus),[147–150] and the motor and somatosensory cortices between the crown and the ear (in response to movements, tactile stimulation, or pain).[151–154] However, many other studies have been reported, including those on the parietal,[155] frontal,[156] temporal,[157] and olfactory[158] lobes.

In most functional imaging experiments, a well-defined stimulus is devised (such as tapping fingers, or watching a pattern or picture). A subject then performs or receives the stimulus at regular or carefully controlled intervals. In almost all cases, data are then processed to isolate signals that correlate with the presentation of the stimulus. In all functional imaging modalities, and especially for higher mammals such as humans, there is always some variability in baseline brain activity during an experiment that can generally only be eliminated by performing repetitive trials and averaging or filtering.

fMRI is rapidly becoming a clinical tool with which to investigate the effects of diseases and drugs, to plan surgeries, and to study brain development.[9] Optical topography is also finding similar clinical applications.[147,163–165]

3.1.2 *Basic principles: near-infrared spectroscopy for topography*

Direct topography. Direct topography is the most widespread approach to clinical optical brain imaging and is often referred to as near-infrared spectroscopy (NIRS). In its sim-

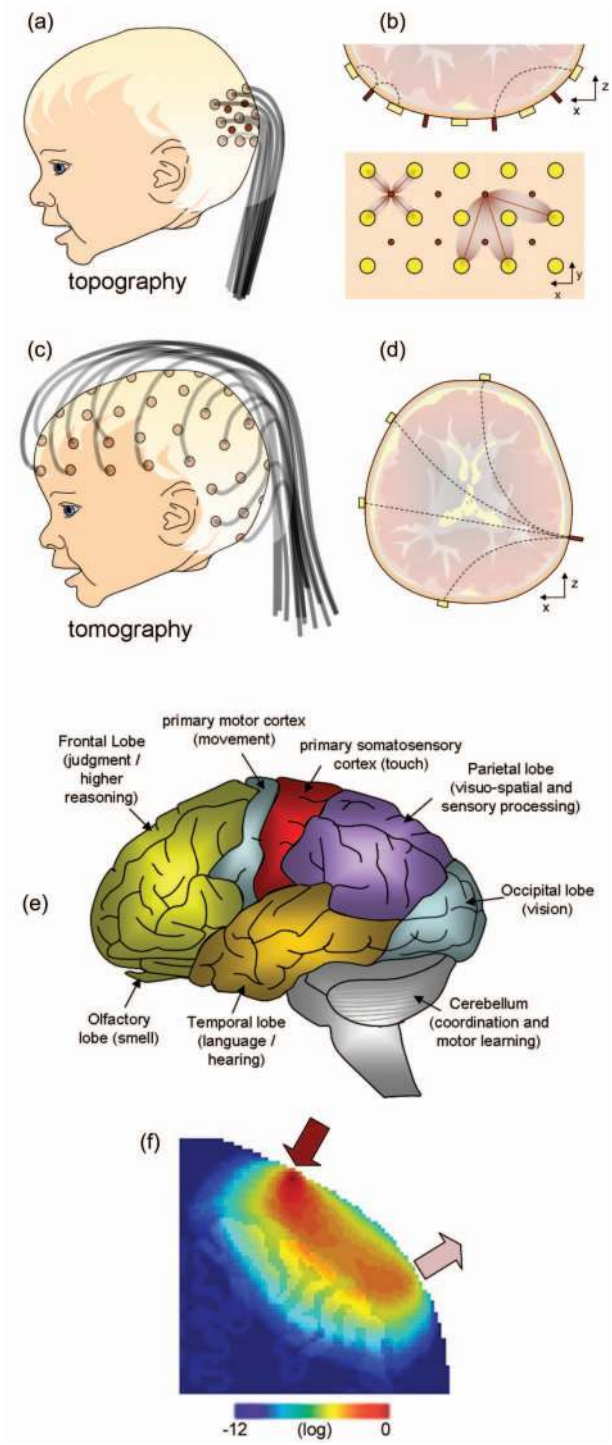

Fig. 5 Configurations for noninvasive optical brain imaging. (a) and (b) Functional topography uses one or more source-detector pairs to create a pseudo-2-D map of the underlying cortex. Sources and detectors may be optical fibers, or light emitting diodes and photodetectors placed directly on the skin. (c) and (d) Tomography places sources and detectors over the volume of the head, and detects light that has traveled through many projections. This approach allows subsequent reconstruction of the optical properties of the entire brain. (e) The main functional areas of the human cortex. (f) Simulation of the sensitivity of a noninvasive topographic measurement between a source and detector. The simulation used Monte-Carlo modeling and accounted for the heterogeneous 3-D structures of the adult scalp and cortex. Reproduced with permission from Boas et al.[202]

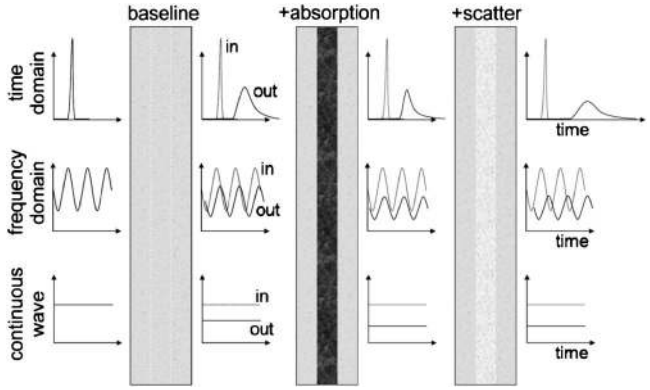

Fig. 6 Time-domain, frequency-domain, and continuous wave measurement sensitivities to absorption and scatter. Schematic shows simplistically how absorbing and scattering structures will change TD and FD data, but that in transmission, their effect on cw data will be indistinguishable.

plest form, NIRS uses light source and detector pairs positioned on the head of infants or adults. Light that passes through the skull scatters within the cortex of the brain [as illustrated in Figs. 1(b), 5(b), and 5(f)]. Despite significant attenuation, variations in absorption due to changes in local HbT, HbO_2, and HbR concentration result in detectable modulations in the intensity of the emerging light. If an array of sources and detectors is used, the changes measured between each source-detector pair can be approximately mapped or interpolated to the underlying cortex, and a low-resolution (>5 mm) 2-D topographical map of cortical activation can be produced.[152,154,173] When many overlapping and multidistance topographic measurements are acquired, it is possible to use mathematical models of light propagation to create a depth-resolved reconstruction of functional activation.[174–176] While more complex, this approach can overcome several of the limitations of direct topography, as described below.

Instrumentation. Noninvasive optical brain imaging instrumentation may be continuous wave (cw), frequency domain (FD), or time domain (TD). cw is the most common approach and simply measures the intensity of light emerging from the head at two or more wavelengths. Data acquisition is often frequency encoded (up to ~kHz), such that multiple wavelengths[177,178] or multiple sources[149,179–181] can be measured simultaneously. FD and TD instruments are substantially more complex and expensive, and can measure both a cw component and the time taken for light to pass through the tissue.[182] FD instruments achieve this by modulating their illumination at around 100 MHz and measuring the phase delay of the emerging light.[152,183] TD instruments use a pulsed laser and measure the temporal distribution of the photons emerging from the tissue.[145,184–188] The main purpose of this temporal information is to provide a measure of the scattering properties of the head, as illustrated in Fig. 6.

Optical fibers are generally used to transmit light to and from the head (see Fig. 5). Direct placement of small sources and detectors on the head has also been demonstrated.[166,189]

Calculation of HbO_2 and HbR concentrations. The change in intensity measured between a topographic source and detector (the attenuation) will generally reflect a change in the

absorption of underlying tissue [Eq. (1)]. The basic approach for deriving changes in HbO_2 and HbR concentration from changes in attenuation was outlined in Sec. 1.1.2 [Eqs. (1) and (5)]. Determining I_0 and G for noninvasive measurements is particularly challenging, since the amount of light coupled into and out of the scalp for every source and detector position would need to be known. Differential measurements relative to time $t=t_0$ [Eq. (3)] should cancel these source- and detector-specific scaling factors, although it must be assumed that these factors stay constant for the duration of the measurement (which can be challenging if the subject moves and/or hair is obstructing probe placement).

As with exposed cortex imaging, if measurements of the change in attenuation at multiple NIR wavelengths are to be converted into changes in hemoglobin concentrations, the effects of scattering must be accounted for. If Eqs. (4) and (5) are to be used for "direct" topography, an estimate of DPF*x* for each wavelength and measurement pair is required.

FD and TD systems can be used to measure DPF*x* directly, and as an adjunct to cw imaging can provide DPF*x* for a given wavelength by measuring the average time taken for light to pass from the source to detector, and converting to distance based on the speed of light in tissue.[190,191] However, if a subset of DPF*x* measurements (or generalized values of DPF) are to be used, it should be noted that DPF*x* could vary depending on age, gender, and even position on the head, owing to the complex structures of the underlying scalp, skull, and convoluted human cortex.

Simulations for calculation of DPF*x* can become increasingly complex if efforts are made to incorporate the curvature of the head, the heterogeneous structures of the scalp, skull, and cortex, the presence of cortical convolutions and sulci, the effects of CSF [see Fig. 1(b)], and even the effects of isotropic scattering in the brain.[88,192–199] Estimates of the absorbing and scattering optical properties of each tissue type,[200,201] as well as accurate knowledge of the source-detector separations between fibers on the head, are also required. If available, an MRI scan of the head can be used to build a customized model of light propagation for each subject, allowing constrained analysis that accommodates the exact structure of the brain, skull, and scalp underlying each detector.[202] However, while this is feasible in studies where fMRI is simultaneously acquired, it is prohibitive for other applications of optical imaging.

Although TD and FD systems rarely have a large number of multiwavelength channels,[161,185] they have the advantage that they can be used to deduce the scattering properties of the head, which can then be incorporated into more complex calculations of hemoglobin concentrations.[201,203] An FD approach is to measure between several source-detector separations and, under simplifying assumptions of homogeneity, fit for scattering and absorption based on a linearized model of light propagation versus distance.[183] Such approaches do not require estimates of DPF*x*.

In general, for direct topography, simplified models and scaling factors are applied to account for DPF*x* and also partial volume effects, which correct for the fact that only a fraction of the detected light actually sampled the cortex.[34,153,159,183,204] Several studies have explored the importance of accurate calculation/measurement of DPF*x* and its impact on the determination of hemoglobin concentrations for optical topography.[198,205,206] It has been shown that in many cases, useful functional information can be obtained even when simplifying assumptions are applied to analysis and interpretation. *However, it is therefore important to consider the possible impact of systematic errors resulting from this analysis for all NIRS measurements, particularly when imaging the adult head, where many confounding effects can obscure cortical signals and impact correct interpretation*.

Extracerebral effects and physiological noise. The effects of blood flow changes in the scalp, and changes in the brain that are not directly related to the cortical stimulus response, must also be considered. The analysis approaches described above assumed that changes in signal were solely due to changes in the cortex of the brain. However, it has also been shown that breathing ($\sim$0.16 Hz), heart rate ($\sim$1 Hz), and the "vasomotor" or Mayer wave signal ($\sim$0.1 Hz)[207–210] can cause large changes in measured hemodynamic signals. Substantial repetition of a stimulus and averaging should reduce the effects of unrelated physiological variations in blood flow in the scalp and brain. However, acquisition of so many repetitions is not always possible with adult or infant subjects. In addition, some responses may not average out, or may intrinsically correlate or become entrained with the stimulus period,[208] and can affect both brain blood flow and the rich blood supply to the scalp. Recent evidence has suggested that certain stimuli actually invoke a systemic response (possibly through heart rate or blood pressure changes) that could manifest as a change in scalp or even baseline cortical blood flow that correlates with the stimulus period.[153,211]

Several measurement, data analysis, and filtering approaches have been proposed to reduce the influence of hemodynamic activity unrelated to the true cortical response. One approach is to simultaneously acquire measurements between close and more distant pairs of sources and detectors, assuming that the closer detector is predominantly detecting signal from the scalp. This scalp signal can then be approximately removed from the signal from the more distant detector, assuming that a similar superficial contribution is affecting both measurements. A similar approach can be achieved with TD data, where the photons arriving at a detector earlier are likely to have traveled more superficially, and therefore contain information about the scalp signal. The benefit of using TD is that later photons that have traveled more deeply between the same source detector travel through the same region of the scalp as the early photons, so cancellation should be improved relative to the multidistance approach.[187,212] An extension of this is reconstructed topography, which creates a depth-resolved map that should be able to spatially separate superficial signals from deeper cortex signals, if suitable measurements are acquired.

Spatiotemporal filtering and modeling have also been proposed as a way to remove these systemic signals.[213,214] While rapidly becoming more sophisticated, implementation of these data processing techniques can be complex and sometimes subjective. Extensive processing could result in distortion of true cortical signals, particularly when attempting to separate scalp and cortical signals that may both have elements correlating with the stimulus response.[211]

Practical measurements. A final difficulty with acquiring functional optical imaging data is reliable placement of sources and detectors on the head. The primary problem is to be able to securely position multiple probes in a pattern such that their interfiber distances are known, and they stay stable during the course of the measurement. Hair on the head is a major challenge, as it can significantly attenuate light entering and leaving the head, and can cause measurement instability over time if the probes shift. Technical advancements have been made in positioning optical fibers and probes onto the head, and relatively stable configurations have been devised.[180] However, further work will be required before it becomes possible to routinely, rapidly, and repeatably position optical topography fibers on the head.

Reconstructed topography. Direct topography is the simplest way to analyze topographic data, but relies on many assumptions and simplifications. An alternative approach is to reconstruct data onto a 3-D rendering of the head. Although analysis becomes more complex, by creating a depth-resolved image of the measured absorption changes, some of the confounds described earlier can be overcome.

Image reconstruction.

Instead of requiring a pathlength estimate, reconstruction effectively attempts to recreate the measured data by simulating alterations in the absorption distribution within the head.[187,215,216] When the simulated data and the measured data match, the absorption distribution is assumed to be correct. Reconstructing still generally requires an estimate of the baseline absorbing and scattering optical properties of the head, and an accurate model of light propagation, but can help if there are depth-dependent variations in the response, including effects from the scalp. Partial volume effects, particularly where one wavelength of light effectively probes a different region, than a second wavelength, can also be accommodated in reconstructed topography.

For reconstructed topography to be effective, it is necessary to measure signals between overlapping sources and detectors, and generally at several source-detector distances [see Fig. 5(b)]. These measurements provide a set of mutually consistent data for which there should be only one possible corresponding differential absorption distribution. This in turn should also lead to improved x-y resolution.[175,176,179]

Modeling of light propagation in the human head typically uses either Monte Carlo modeling or the diffusion approximation (DA) to the radiative transfer equation [Eq. (6)] and a linearizing assumption such as the Born [Eq. (7)] or Rytov approximations.

$$\mu_a \Phi - \nabla \cdot \frac{1}{3(\mu_a + \mu_s')} \nabla \Phi = q_0, \tag{6}$$

$$\Delta M_{n,m} = J_{n,m}(r) \Delta \mu_a(r), \tag{7}$$

where Φ is the photon density within the tissue, and q_0 is the source function. $\Delta M_{n,m}$ is the set of changes in measurement (from time $t=0$) between source n and detector m, and $J_{n,m}(r)$ is the Jacobian matrix derived from the Greens function solution to Eq. (6), representing the change in measurement $\Delta M_{n,m}$ corresponding to a change in absorption μ_a at position r within the tissue.[215] An example of $J_{n,m}(r)$ for a single source-detector pair is shown in Fig. 5(f). This distribution was calculated using a Monte Carlo model of light propagation in a realistic 3-D model of the adult head, based on a segmented MRI scan.[202]

Analytical solutions to the DA for simple shapes such as slabs and semi-infinite planes exist.[197] More complex approaches include applying the DA via finite element or finite difference methods, where heterogeneous structures can be incorporated into the simulation. Monte Carlo modeling can also be used to simulate light propagation in the head, although for large tissue volumes, it can be prohibitively slow. Once the model has been used to generate the Jacobian $J_{n,m}(r)$ (otherwise known as the spatial sensitivity matrix, weight matrix, or photon measurement density function), Eq. (7) can be solved for $\Delta \mu_a$ using a linear inversion technique such as Tikhonov regularization, or more complex nonlinear iterative algorithms.[217]

Plots of $J_{n,m}(r)$ [Fig. 5(f)] reveal the varying paths of light traveling from source to detector, and show how only some of the detected light has sampled the cortex. The areas of highest sensitivity are directly below the source and detector, revealing why changes in coupling and the scalp have such a significant effect on signal amplitude. The banana shape of the light path is characteristic of diffuse imaging, and is maintained as source-detector distances get larger or smaller, such that the center region gets deeper or shallower, respectively.

Implementation of reconstructed topography can be achieved with various levels of complexity. The simplest approach assumes that changes in absorption are occurring in a homogenous volume of known optical properties. This is an approximation, since the baseline structures of the skull and brain will affect the shape of $J_{n,m}(r)$ [as shown in Fig. 5(f)] in a way that cannot be accounted for in a homogenous model.[198,218,219] The effects of CSF have also been widely considered, since the diffusion approximation is only valid for scattering regions where $\mu_s' \gg \mu_a$, which is not likely to be true for large thicknesses of CSF.[196,199] Several papers further suggested that light piping could occur in the CSF layer, significantly reducing penetration of light into the cortex. However, more recent publications have questioned the magnitude of the effect once the complex 3-D nature of the CSF layer, trabeculi, vessels, and refractive index differences are taken into account.[193,194,217] By incorporating *a priori* structural information into the image reconstruction scheme, constraints can be applied to help improve the localization of activation to the cortex, although care must be taken to account for changes in the data that may originate from extra-cerebral contributions.[202]

Data acquisition. As NIR light sources and detectors become increasingly affordable, it has become possible to construct NIRS instruments with large numbers of multiwavelength source and detector channels. While larger arrays allow simultaneous mapping of several regions of the cortex simultaneously, they also present significant challenges for fast data acquisition.[180] Since the human heart beat causes substantial variations in NIRS signals,[220] aliasing can be a significant problem unless measurements from all source-detectors pairs can be acquired at a rate of at least 2 Hz. Systems that utilize frequency encoding to allow all sources to be illuminated simultaneously can acquire data in parallel at high frame

rates.[152,181] However, the attenuation difference between a source and detector separated by 2.5 and 4.25 cm can be up to two orders of magnitude.[179] For reconstructed topography, these multidistance measurements are vital, and detectors must have excellent dynamic range and noise characteristics to be able to simultaneously distinguish between frequency-encoded signals of such varying amplitudes. Development of faster systems, with better dynamic range or highly advanced and rapid multiplexing schemes is therefore ongoing.[176,179]

3.2 *Tomography*

The most complex approach to optical brain imaging involves performing a full 3-D reconstruction of the entire head using an approach similar to x-ray computed tomography. This approach has only been demonstrated on small infants, since it requires light to be transmitted across the whole head [as shown in Figs. 5(d)].[145,221–223] However, the benefits are that in addition to functional imaging, this approach can potentially enable imaging of pathologies such as periventricular hemorrhage and ischemia in a perinatal setting, where currently no alternative diagnostic and monitoring tools are available.[217]

3.2.1 *Basic principles*

Since the use of 3-D tomography for brain imaging is not yet widespread, specific details of one study are given in the next section, and only a brief overview is provided here.

For tomographic imaging, it is necessary to acquire a series of measurements or projections through the tissue being imaged. For reconstructed topography, measurements between sources and detectors with different separations allow some depth-resolved information to be deduced. In tomography, the same basic image reconstruction approach is used, but a larger number of projections through the head at different angles are required to calculate the 3-D structure deep within the brain [see Figs. 5(c) and 5(d)]. Note that optical tomography has also been used to image the adult breast for the detection or monitoring of breast cancer[224] and the human forearm.[225]

There are three main difficulties with acquiring tomographic data on the head. The first is that light must be detected through greater than 7 cm of tissue, which in general will cause around 10^{-7} attenuation of the incident light. The second difficulty is that the paths of light through the head are again a function of baseline anatomical structures. Third, to look at pathologies or regions of ischemia for which a baseline (e.g., prestimulus state) is not available, it can be valuable to attempt to reconstruct this absolute absorbing and scattering structure of the brain, and not just measure changes (as with topography).

3-D tomographic imaging of the neonatal had has been demonstrated using TD instruments.[145,222,223] TD measurements that use single photon counting have the advantage that very low light levels can be detected by increasing measurement integration time. Background signal and thermal noise will not be temporally correlated, and can often be subtracted from the true signal.[226] Therefore, while slow, TD systems can detect usable signals across 15 cm of adult breast, or an entire neonatal infant's head. TD and FD measurements also have the benefit that they allow the effects of scatterers and absorbers to be distinguished (as illustrated in Fig. 6,[215,227] although see (Ref. 228). In fact, using TD data, it is possible to reconstruct images of both absolute baseline absorbing *and* scattering structures.[229] These methods are currently being developed to allow imaging of the baseline optical properties of the infant brain.

Differential measurements can be used to reconstruct absorption changes, under the same assumptions as topography: that scattering does not change and the effects of heterogeneous background absorbing and scattering structure on light paths is insignificant or can be incorporated into a model of the head.[217,219] Differential imaging of 3-D absorption changes can be achieved with relatively simple linearized reconstruction approaches similar to those used for reconstructed topography described before.[217,222] Values of $J_{n.m}(r)$ must be calculated based on the 3-D shape of the head, and the precise positions of the sources and detectors [see Fig. 5(c)]. Typically, this is done using finite element models implementing the diffusion approximation, and sometimes incorporating estimates of the baseline absorbing and scattering structures within the head.[230,231]

For absolute imaging of the baseline absorbing and scattering structure of the brain, a nonlinear algorithm should be used that iteratively seeks a 3-D distribution of absorbing and scattering that can account for the data measured on the head. A highly complex and publicly available software package developed to do both nonlinear reconstruction of absorption and scattering images, as well as forward modeling of $J_{n.m}(r)$ using the finite element method is called TOAST (time-resolved optical absorption and scattering tomography).[215,232,233]

The data that are actually fed into these reconstruction algorithms will have a significant effect on image sensitivity to scatter and absorption.[217] FD data consists of measurements of amplitude and phase. Measurements are typically made at modulation frequencies between 100 and 200 MHz.[234] TD data represents the full impulse response of the tissue, and therefore amplitude and phase at almost any effective modulation frequency can be calculated. Datatypes such as the mean-time or integrated intensity of the signal can also be extracted.[226] For images of both absorption and scatter, the image reconstruction algorithm must utilize both amplitude and phase data, or at least two sufficiently different time-resolved parameters. A very accurate model of light propagation and precise calibration of data for systematic errors is also very important, particularly if absolute images of absorption and scatter are required (since the data must closely match simulated data corresponding to the correct 3-D distribution of absorption and scatter).[217,226]

3.3 *Examples of Noninvasive Optical Brain Imaging*

Figure 7 shows a variety of noninvasive optical brain imaging results showing human functional responses to stimulus. Figure 7(a) shows results from a study using cw direct topography to examine the hemodynamic response to different kinds of stimuli: finger tapping, median nerve electrical stimulation, and tactile stimulation.[153] Stimuli were presented for 10 sec, followed by 18 sec of rest, and were repeated 20 times per subject. The cw system has 16 laser diode sources, eight at 690 nm and eight at 830 nm, frequency encoded between 4

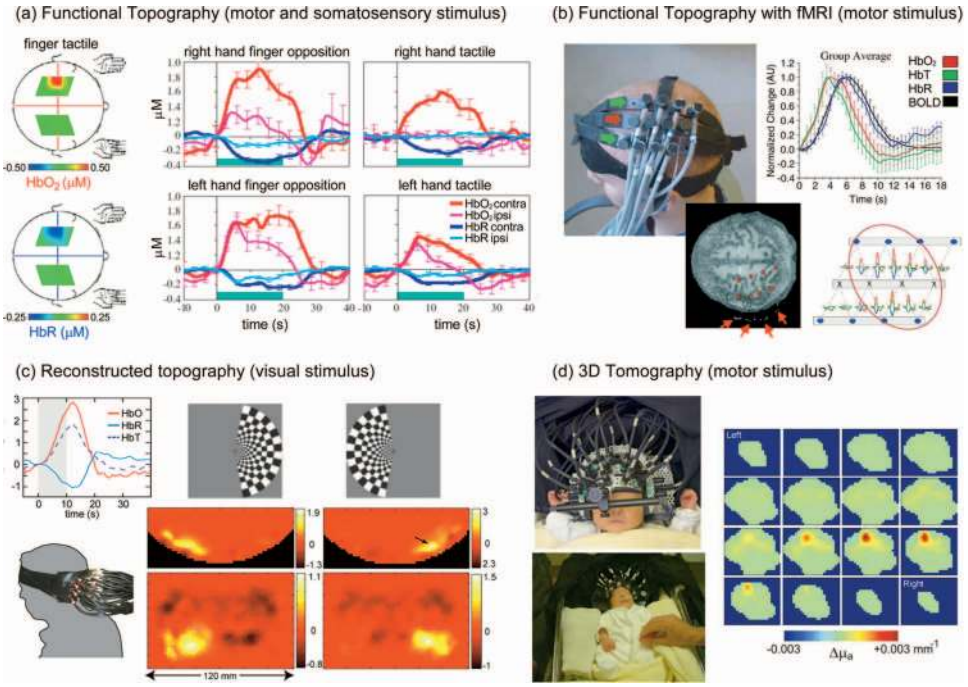

Fig. 7 Examples of noninvasive optical imaging of functional responses in humans. (a) Direct functional topography images and time courses acquired for two different motor/somatosensory stimulus paradigms on one subject. A localized HbO_2 and HbR response is seen in the opposite (contralateral) side of the brain to the hand being stimulated. Reproduced with permission from Franceschini et al.[153] (b) Functional topography measurements on adult head during fMRI. Both the spatial and temporal characteristics of the responses can be compared between two modalities. Reproduced with permission from Huppert et al.[159] (c) Black and white visual stimuli were presented to the left and right fields of vision. The hemodynamic response was measured using a dense topographic array of sources and detectors. Data were reconstructed using a linear perturbation model. Reproduced with permission from Culver et al.[176] (d) Time-resolved 3-D tomography data were acquired on a 33-week gestation infant undergoing passive motor stimulus to the left arm. Image series shows successive slices through 3-D head from left ear to right ear. Reproduced with permission from Gibson et al.[222]

and 7.4 kHz such that all were illuminated while 16 avalanche photodiode detectors collected emerging light. Sources and detectors were configured in two panels, arranged as shown in the photograph in Fig. 7(b) where four fibers span the center (each delivering both 690 and 830 nm—red arrow), straddled by two rows of four detector fibers—green arrows. The detected signal was digitized at 40 kHz and analyzed to extract signals coming only from the closest sources (3 cm) to each detector. Data were then low-pass filtered and downsampled to 10 Hz, and then bandpass filtered between 0.02 and 0.5 Hz to eliminate heart beat pulsations and slow drifts. Data were then block averaged over the 20 trials to reveal the average attenuation changes corresponding to each stimulus. These attenuation values were converted to absorption changes using literature values of the differential pathlength factor DPF at 690 nm (6.51) and 830 nm (5.86), such that the pathlength is DPFx, where x is the source-detector separation of 3 cm. The resulting absorption changes were then converted to HbO_2 and HbR changes using Eq. (4). These source-detector-specific changes in hemodynamics were then projected onto a map underneath each source-detector pair using an approximate weighted spatial distribution based on the volume sampled. The final map was then interpolated onto a finer grid. The images and time courses in Fig. 7(a) show the mean maps and time courses for a single subject. Contralateral responses are those seen in the side of the brain opposite the hand receiving the stimulus (where responses would be expected).

Figure 7(b) shows a similar study, but where optical topography data were acquired during simultaneous fMRI at 3 tesla.[159] The subjects performed a finger tapping exercise for 2 sec, with a randomized interstimulus interval between 4 and 20 sec repeated between 27 and 32 times per fMRI scan, with each scan repeated four to six times. fMRI scans with a 2-Hz frame rate were used to measure either BOLD contrast or ASL data, which provides blood flow information. The cw NIRS instrument and data processing approach was similar for this and the study described previously.[153] The HbO_2, HbR, and HbT time courses for one subject and for each source-detector pair are shown in map form [inset lower right of Fig. 7(b)]. Oil-filled fiducials on the optical fiber heads allowed the optical probe's location to be coregistered with the MRI scans. The time course of the fMRI BOLD signal is compared to the HbO_2, HbR, and HbT temporal responses measured using NIRS. The group average of five subjects is shown, and the work concludes that BOLD most closely temporally correlates with HbR changes. ASL changes were found to correlate most closely with HbT changes (data not shown). A second paper continues this analysis to a spatial comparison between the localization of HbR and BOLD responses.[235]

Figure 7(c) shows a reconstructed topography result, acquired on the adult head during a 10 sec visual stimulus followed by 35 sec of darkness.[176] Data were acquired with a multichannel cw NIRS system consisting of 24 radio frequency encoded light-emitting diode (LED) sources at 760 and 850 nm, and 28 avalanche photodiode detectors. Frequency encoding allowed simultaneous acquisition at both wavelengths, but LEDs were switched on sequentially allowing detectors with 10^7 dynamic range to measure signals from sources at three different separations: 13.3, 30.0, and 40.0 mm. Despite this serial source switching, full images were acquired at 10 frames per sec. Data were then reconstructed by inverting the linear problem [Eq. (7)] and using $J_{n.m}(r)$ functions calculated using a finite element model simulation package called NIRFAST,[236] which incorporates a simplified baseline structure consisting of a 15-mm scalp/skull layer (μ_a=0.17 cm^{-1}, μ_s'=7.6 cm^{-1}) surrounding the brain of radius=65 mm (μ_a=0.19 cm^{-1}, μ_s'=11.5 cm^{-1}). Both block averaged and even trial-by-trial data show clear hemodynamic responses to unilateral visual stimulus.

Figure 7(d) shows 3-D optical tomography images of the functional response to passive motor stimulus of the left arm in the brain of a premature infant.[222] The image series represents vertical slices through the 3-D volume of the head (from left ear to right ear). A clear volume of absorption increase is seen in the region corresponding to the right motor cortex. Data were acquired using a dual wavelength, 32-channel time-resolved optical tomography system known as MONSTIR.[186] The images in Fig. 7(d) show the change in absorption at 780 nm, but simultaneously acquired images at 815 nm were also created and converted into maps of the change in HbO_2, HbR, and HbT.Four sleeping premature infants were measured, born at a median gestation of 28 weeks and 5 days, and imaged at a median gestational age of 34 weeks 5 days. Optical fibers were positioned on the head using a custom-made foam-lined semi-rigid cap, shaped to allow careful but stable positioning of many fibers over the full cranium.[217] Since time-resolved data can be slow to acquire, motor stimulus data were collected one source at a time for up to 12 source positions. Each source was illuminated, and the time-resolved transmitted light signal then collected at up to 32 detector positions for 10 sec while the infant rested. The left arm was then gently moved back and forth by an adult for 15 sec, with transmitted light being measured for the last 10 sec of this exercise to capture the resultant hemodynamic response. The next source position was then illuminated, and the 10 sec rest/15 sec exercise cycle repeated.

The resulting time-resolved data were Fourier transformed and the log(amplitude) and phase components extracted at 100 MHz. The difference in the log(amplitude) and phase measurements between the active and resting states effectively cancels out errors relating to optical coupling and the system's impulse response function.[217,225,226] The resulting differential measurements were then reconstructed into a 3-D map of absorption changes. In this case, a linearized model similar to Eq. (7) was utilized with careful normalization and scaling, and compensation for errors in optical coupling incorporated into Tikhonov inversion.[237] The $J_{n.m}(r)$ functions were generated using a finite element model implementing the diffusion equation in a homogenous 3-D volume corresponding to the contours of the infant's head. The MONSTIR system and finite element algorithm (TOAST) have been used for a number of other 3-D optical tomography imaging studies on premature infants.[145,223,238]

3.4 *Methodological Extras*

3.4.1 *Cytochrome oxidase*

Significant efforts have been made to topographically measure changes in a third intrinsic brain chromophore called cytochrome oxidase. Cytochrome oxidase is a mitochondrial enzyme that plays an important role in oxygen metabolism in the brain. Cytochrome does not change its concentration, but changes its oxidation state (and absorption spectrum) during the production of adenosine triphosphate (ATP). The concentration of cytochrome oxidase in the brain is lower than that of hemoglobin (2 to 3 micromolar compared to 40 to 60 micromolar), so based on published spectra, the peak absorption in brain of reduced cytochrome C would be $<$0.06 cm^{-1} at 550 nm, changing to 0.017 cm^{-1} when oxidized, and 0.00064 to 0.0002 cm^{-1} at 800 nm (compare to equivalent hemoglobin spectra in Fig. 1).[239] It is therefore very desirable, but quite difficult to measure changes in the redox state of cytochrome oxidase *in vivo*. Nevertheless, measurement methods have been studied carefully[240–242] and NIRS-based cytochrome measurements have been reported in adults.[209,243]

Exogenous dyes for noninvasive imaging. Exogenous contrast agents can also be used for noninvasive brain imaging. Indocyanine green (ICG) is an FDA-approved dye commonly used for liver and cardiac function tests.[244] ICG has strong NIR absorption and fluorescence, and does not cross the blood brain barrier, and so has also found several optical brain imaging applications. A bolus of ICG can be used to quantify blood flow in the brain, by observing the rate of arrival and accumulation of the dye with NIRS measurements.[245] Changes in the dynamics of a dye bolus in patients with perfusion abnormalities such as thrombolitic stroke have also been studied using NIRS.[246] ICG has been used to simultaneously determine cerebral blood volume and total circulating blood volume in neonates undergoing blood transfusions.[247] An interesting recent study reported that it was possible to also observe the fluorescence of ICG in the brain using noninvasive NIRS.[248] This result is important as it supports the possibility that more specifically targeted long-wavelength dyes could feasibly be measured noninvasively in the brain. Such molecular probes may have sufficient specificity to allow localization or even diagnosis of diseases such as brain cancer and Alzheimer's.[139,249]

Noninvasive neuronal imaging via fast scattering. Since it is not possible to use voltage-sensitive dyes in humans, researchers are highly motivated to isolate a strong source of contrast that can directly report changes in neuronal activity. Observation of the fast scattering signal in exposed rodent cortex was described in Sec. 2.1.4. Noninvasive measurement of this signal is highly challenging, as scattering changes are difficult to detect accurately and separate from the effects of absorption. Recent studies of the fast scattering signal have shown compelling results, and compared findings to EEG and fMRI.[161,250,251] However, it is still questioned whether the fast signal is sufficiently robust for routine measurement.[104,105]

Diffuse correlation spectroscopy. A relatively recent addi-

tion to optical topography has been the development of diffuse correlation spectroscopy (DCS), which allows noninvasive measurement of cortical blood flow. The theoretical basis of this technique is similar to that of speckle-flow imaging described in Sec. 2.1.2, but DCS measures the temporal autocorrelation of laser light with a long coherence length that has scattered through tissue containing moving red blood cells. For human imaging, DCS acquires signals through single mode fibers placed on the scalp.[252–254] Promising results in humans have been reported,[255] and it has been shown that it is possible to extend the technique to allow 3-D imaging.[256]

4 Summary

We have reviewed a wide range of approaches to optical brain imaging, and explored their many important applications to neuroscience. We have provided insights into the fundamental basis of many optical imaging techniques, and highlighted important considerations for their practical implementation. We hope that these details will enable those interested in adopting or developing optical imaging methods to understand the key aspects that should be considered when acquiring measurements or analyzing data.

We have sampled the huge body of literature that has successfully used optical brain imaging in all its forms for ground-breaking and fundamentally important research and applications. It is clear that optical brain imaging is a rapidly expanding field, continually evolving to embrace new technologies, contrast mechanisms, and *in-vivo* applications.

Acknowledgments

The author acknowledges the help of Matthew B. Bouchard and Sean A. Burgess in proof reading this manuscript, as well as the help and support of many at the Athinoula A. Martinos Center for Biomedical Imaging, Massachusetts General Hospital. Funding was provided by NIH/NINDS grant R21NS053684, NIH/NHLBI grant R01HL071635, and the Wallace Coulter Foundation.

References

1. F. F. Jöbsis, "Non invasive, infrared monitoring of cerebral and myocardial oxygen sufficiency and circulatory parameters," *Science* **198**, 1264–1267 (1977).
2. D. Shoham, D. E. Glaser, A. Arieli, T. Kenet, C. Wijnbergen, Y. Toledo, R. Hildesheim, and A. Grinvald, "Imaging cortical dynamics at high spatial and temporal resolution with novel blue voltage-sensitive dyes," *Neuron* **24**, 791–802 (1999).
3. K. Ohki, S. Chung, Y. H. Ch'ng, P. Kara, and R. C. Reid, "Functional imaging with cellular resolution reveals precise micro-architecture in visual cortex," *Nature (London)* **433**, 597–603 (2005).
4. M. I. Kotlikoff, "Genetically encoded Ca2+ indicators: using genetics and molecular design to understand complex physiology," *J. Physiol. (London)* **578**(Pt 1), 55–67 (2007).
5. W. E. Klunk, B. J. Bacskai, C. A. Mathis, S. T. Kajdasz, M. P. Frosch, M. L. Debnath, D. P. Holt, Y. Wang, and B. T. Hyman, "Imaging Aβ plaques in living transgenic mice with multiphoton microscopy and methoxy-X04, a systemically administered Congo red derivative," *J. Neuropathol. Exp. Neurol.* **61**(9), 797–805 (2002).
6. S. Ogawa, T. M. Lee, A. R. Kay, and D. W. Tank, "Brain magnetic resonance imaging with contrast dependent on blood oxygenation," *PNAS* **87**(24), 9868–9872 (1990).
7. J. W. Belliveau, D. N. Kennedy, R. C. McKinstry, B. R. Buchbinder, R. M. Weisskoff, M. S. Cohen, J. M. Vevea, T. J. Brady, and B. R. Rosen, "Functional mapping of the human visual cortex by magnetic resonance imaging," *Science* **254**(5032), 716–719 (1991).
8. K. K. Kwong, J. W. Belliveau, D. A. Chesler, I. E. Goldberg, R. M. Weisskoff, B. P. Poncelet, D. N. Kennedy, B. E. Hoppel, M. S. Cohen, R. Turner, H-M Cheng, T. J. Brady, and B. R. Rosen, , "Dynamic magnetic resonance imaging of human brain activity during primary sensory stimulation," *Proc. Natl. Acad. Sci. U.S.A.* **89**(12), 5675–5679 (1992).
9. P. M. Matthews, G. D. Honey, and E. T. Bullmore, "Applications of fMRI in translational medicine and clinical practice," *Nat. Rev. Neurosci.* **7**(9), 732–744 (2006).
10. D. S. Williams, J. A. Detre, J. S. Leigh, and A. P. Koretsky, "Magnetic resonance imaging of perfusion using spin inversion of arterial water," *Proc. Natl. Acad. Sci. U.S.A.* **89**(1), 212–216 (1992).
11. J. B. Mandeville, J. J. Marota, B. E. Kosofsky, J. R. Keltner, R. Weissleder, B. R. Rosen, and R. M. Weisskoff, "Dynamic functional imaging of relative cerebral blood volume during rat forepaw stimulation," *Magn. Reson. Med.* **39**(4), 615–624 (1998).
12. J. B. Mandeville, J. J. Marota, C. Ayata, M. A. Moskowitz, R. M. Weisskoff, and B. R. Rosen, "MRI measurement of the temporal evolution of relative CMRO(2) during rat forepaw stimulation," *Magn. Reson. Med.* **42**(5), 944–951 (1999).
13. C. Ayata, A. K. Dunn, Y. Gursoy-Özdemir, Z. Huang, D. A. Boas, and M. A. Moskowitz, "Laser speckle flowmetry for the study of cerebrovascular physiology in normal and ischemic mouse cortex," *J. Cereb. Blood Flow Metab.* **24**, 744–755 (2004).
14. T. L. Spires, M. Meyer-Luehmann, E. A. Stern, P. J. McLean, J. Skoch, P. T. Nguyen, B. J. Bacskai, and B. T. Hyman, "Dendritic spine abnormalities in amyloid precursor protein transgenic mice demonstrated by gene transfer and intravital multiphoton microscopy," *J. Neurosci.* **25**, 7278–7287 (2005).
15. H. Bolay, U. Reuter, A. Dunn, D. Boas, and M. Moskowitz, "Intrinsic brain activity triggers trigeminal meningeal afferents in a migraine model," *Nat. Med.* **8**, 136–142 (2002).
16. S. Bahar, M. Suh, M. Zhao, and T. H. Schwartz, "Intrinsic optical signal imaging of neocortical seizures: the 'epileptic dip'," *NeuroReport* **17**(5), 499–503 (2006).
17. J. Berwick, I. M. Devonshire, A. J. Martindale, D. Johnston, Y. Zheng, A. J. Kennerley, P. G. Overton, and J. E. Mayhew, "Cocaine administration produces a protracted decoupling of neural and haemodynamic responses to intense sensory stimuli," *Neuroscience (Oxford)* **132**(2), 361–374 (2005).
18. A. Devor, A. K. Dunn, M. L. Andermann, I. Ulbert, D. A. Boas, and A. M. Dale, "Coupling of total hemoglobin concentration, oxygenation, and neural activity in rat somatosensory cortex," *Neuron* **39**(2), 353–359 (2003).
19. E. M. C. Hillman, A. Devor, M. Bouchard, A. K. Dunn, G. W. Krauss, J. Skoch, B. J. Bacskai, A. M. Dale, and D. A. Boas, "Depth-resolved optical imaging and microscopy of vascular compartment dynamics during somatosensory stimulation," *Neuroimage* **35**(1), 89–104 (2007).
20. N. Pouratian, A. F. Cannestra, N. A. Martin, and A. W. Toga, "Intraoperative optical intrinsic signal imaging: a clinical tool for functional brain mapping," *Neurosurg. Focus* **13**(4), e1 (2002).
21. A. F. Cannestra, N. Pouratian, S. Y. Bookheimer, N. A. Martin, D. P. Beckerand, and A. W. Toga, "Temporal spatial differences observed by functional MRI and human intraoperative optical imaging," *Cereb. Cortex* **11**(8), 773–782 (2001).
22. M. Suh, S. Bahar, A. D. Mehta, and T. H. Schwartz, "Blood volume and hemoglobin oxygenation response following electrical stimulation of human cortex," *Neuroimage* **31**(1), 66–75 (2006).
23. C. Martin, J. Martindale, J. Berwick, and J. Mayhew, "Investigating neural-hemodynamic coupling and the hemodynamic response function in the awake rat," *Neuroimage* **32**(1), 33–48 (2006).
24. H. Slovin, A. Arieli, R. Hildesheim, and A. Grinvald, "Long-term voltage-sensitive dye imaging reveals cortical dynamics in behaving monkeys," *Neurophysiology* **88**(6), 3421–3438 (2002).
25. A. M. Dale, "Optimal experimental design for event-related fMRI," *Hum. Brain Mapp* **8**(2–3), 109–114 (1999).
26. C. W. Roy and C. S. Sherrington, "On the regulation of the blood supply of the brain," *J. Physiol. (London)* **11**, 85–108 (1890).
27. D. Y. Ts'o, R. D. Frostig, E. E. Lieke, and A. Grinvald, "Functional organization of primate visual cortex revealed by high resolution optical imaging," *Science* **249**(4967), 417–420 (1990).
28. R. D. Frostig, E. E. Lieke, D. Y. Ts'o, and A. Grinvald, "Cortical functional architecture and local coupling between neuronal activity and the microulation revealed by in vivo high-resolution optical im-

aging of intrinsic signals," *Proc. Natl. Acad. Sci. U.S.A.* **87**, 6082–6086 (1990).
29. I. Vanzetta, R. Hildesheim, and A. Grinvald, "Compartment-resolved imaging of activity-dependent dynamics of cortical blood volume and oximetry," *J. Neurosci.* **25**(9), 2233–2244 (2005).
30. A. Dunn, A. Devor, M. Andermann, H. Bolay, M. Moskowitz, A. Dale, and D. Boas, "Simultaneous imaging of total cerebral hemoglobin concentration, oxygenation and blood flow during functional activation," *Opt. Lett.* **28**, 28–30 (2003).
31. J. Berwick, D. Johnston, M. Jones, J. Martindale, P. Redgrave, N. McLoughlin, I. Schiessl, and J. E. W. Mayhew, "Neurovascular coupling investigated with two-dimensional optical imaging spectroscopy in rat whisker barrel cortex," *Eur. J. Neurosci.* **22**(7), 1655–1666 (2005).
32. J. Mayhew, D. Johnston, J. Berwick, M. Jones, P. Coffey, and Y. Zheng, "Spectroscopic analysis of neural activity in brain: increased oxygen consumption following activation of barrel cortex," *Neuroimage* **12**(6), 664–675 (2000).
33. D. Malonek and A. Grinvald, "Interactions between electrical activity and cortical microulation revealed by imaging spectroscopy: implications for functional brain mapping," *Science* **272**, 551–554 (1996).
34. M. Cope, "The application of near infrared spectroscopy to non invasive monitoring of cerebral oxygenation in the newborn infant," in *Department of Medical Physics and Bioengineering*, p. 342, Univ. College London, London (1991).
35. M. Kohl, U. Lindauer, G. Royl, M. Kuhl, L. Gold, A. Villringer, and U. Dirnagl, "Physical model for the spectroscopic analysis of cortical intrinsic optical signals," *Phys. Med. Biol.* **45**, 3749–3764 (2000).
36. A. K. Dunn, A. Devor, A. M. Dale, and D. A. Boas, "Spatial extent of oxygen metabolism and hemodynamic changes during functional activation of the rat somatosensory cortex," *Neuroimage* **27**(2), 279–290 (2005).
37. M. Jones, J. Berwick, D. Johnston, and J. Mayhew, "Concurrent optical imaging spectroscopy and laser-Doppler flowmetry: the relationship between blood flow, oxygenation, and volume in rodent barrel cortex," *Neuroimage* **13**, 1002–1015 (2001).
38. N. Hewson-Stoate, M. Jones, J. Martindale, J. Berwick, and J. Mayhew, "Further nonlinearities in neurovascular coupling in rodent barrel cortex," *Neuroimage* **24**, 565–574 (2005).
39. S. A. Sheth, M. Nemoto, M. Guiou, M. Walker, N. Pouratian, and A. W. Toga, "Linear and nonlinear relationships between neuronal activity, oxygen metabolism, and hemodynamic responses," *Neuron* **42**, 347–355 (2004).
40. C. Iadecola, "Neurovascular regulation in the normal brain and in Alzheimer's disease," *Nat. Rev.* **5**, 347–360 (2004).
41. H. Girouard and C. Iadecola, "Neurovascular coupling in the normal brain and in hypertension, stroke, and Alzheimer disease," *J. Appl. Physiol.* **100**(1), 328–335 (2006).
42. I. Tasaki, A. Watanabe, R. Sandlin, and L. Carnay, "Changes in fluorescence, turbidity and birefringence associated with nerve excitation," *PNAS* **61**, 883–888 (1968).
43. H. S. Orbach, L. B. Cohen, and A. Grinvald, "Optical mapping of electrical activity in rat somatosensory and visual cortex," *J. Neurosci.* **5**(7), 1886–1895 (1985).
44. A. Grinvald, E. Lieke, R. D. Frostig, C. D. Gilbert, and T. N. Wiesel, "Functional architecture of cortex revealed by optical imaging of intrinsic signals," *Nature (London)* **324**, 361–364 (1986).
45. A. Grinvald, "Real-time optical mapping of neuronal activity: from single growth cones to the intact mammalian brain," *Annu. Rev. Neurosci.* **8**, 263–305 (1985).
46. C. C. H. Petersen and B. Sakmann, "Functionally independent columns of rat somatosensory barrel cortex revealed with voltage-sensitive dye imaging," *J. Neurosci.* **21**(21), 8435–8446 (2001).
47. C. C. H. Petersen, T. T. G. Hahn, M. Mehta, A. Grinvald, and B. Sakmann, "Interaction of sensory responses with spontaneous depolarization in layer 2/3 barrel cortex," *PNAS* **100**(23), 13638–13643 (2003).
48. W. T. Baxter, J. M. Davidenko, L. M. Loew, J. P. Wuskell, and J. Jalife, "Technical features of a CCD video camera system to record cardiac fluorescence data," *Ann. Biomed. Eng.* **25**(4), 713–725 (1997).
49. S. F. Mironov, F. J. Vetter, and A. M. Pertsov, "Fluorescence imaging of cardiac propagation: spectral properties and filtering of optical action potentials," *Am. J. Physiol. Heart Circ. Physiol.* **291**(1), H327–335 (2006).
50. L. M. Loew, S. Scully, L. Simpson, and A. S. Waggoner, "Evidence for a charge-shift electrochromic mechanism in a probe of membrane potential," *Nature (London)* **281**(5731), 497–499 (1979).
51. D. Smetters, A. Majewska, and R. Yuste, "Detecting action potentials in neuronal populations with calcium imaging," *Methods* **18**(2), 215–221 (1999).
52. D. Derdikman, R. Hildesheim, E. Ahissar, A. Arieli, and A. Grinvald, "Imaging spatiotemporal dynamics of surround inhibition in the barrels somatosensory cortex," *J. Neurosci.* **23**(8), 3100–3105 (2003).
53. C. C. Petersen, A. Grinvald, and B. Sakmann, "Spatiotemporal dynamics of sensory responses in layer 2/3 of rat barrel cortex measured in vivo by voltage-sensitive dye imaging combined with whole-cell voltage recordings and neuron reconstructions," *J. Neurosci.* **23**(4), 1298–1309 (2003).
54. E. Fluhler, V. G. Burnham, and L. M. Loew, "Spectra, membrane binding and potentiometric responses of new charge shift probes," *Biochemistry* **24**, 5749–5755 (1985).
55. C. Stosiek, O. Garaschuk, K. Holthoff, and A. Konnerth, "In vivo two-photon calcium imaging of neuronal networks," *PNAS* **100**(12), 7319–7324 (2003).
56. A. K. Dunn, H. Bolay, M. A. Moskowitz, and D. A. Boas, "Dynamic imaging of cerebral blood flow using laser speckle," *J. Cereb. Blood Flow Metab.* **21**, 195–201 (2001).
57. T. Durduran, M. G. Burnett, G. Yu, C. Zhou, D. Furuya, A. G. Yodh, J. A. Detre, and J. H. Greenberg, "Spatiotemporal quantification of cerebral blood flow during functional activation in rat somatosensory cortex using laser-speckle flowmetry," *J. Cereb. Blood Flow Metab.* **24**(5), 518–525 (2004).
58. A. Devor, I. Ulbert, A. K. Dunn, S. N. Narayanan, S. R. Jones, M. L. Andermann, D. A. Boas, and A. M. Dale, "Coupling of the cortical hemodynamic response to cortical and thalamic neuronal activity," *Proc. Natl. Acad. Sci. U.S.A.* **102**(10), 3822–3827 (2005).
59. J. P. Erinjeri and T. A. Woolsey, "Spatial integration of vascular changes with neural activity in mouse cortex," *J. Cereb. Blood Flow Metab.* **22**(3), 353–60 (2002).
60. R. V. Harrison, N. Harel, H. Hamrahi, J. Panesar, N. Mori, and R. J. Mount, "Local haemodynamic changes associated with neural activity in auditory cortex," *Acta Oto-Laryngol.* **120**(2), 255–258 (2000).
61. C. Gias, N. Hewson-Stoate, M. Jones, D. Johnston, J. E. Mayhew, and P. J. Coffey, "Retinotopy within rat primary visual cortex using optical imaging," *Neuroimage* **24**(1), 200–206 (2005).
62. A. Das and C. D. Gilbert, "Topography of contextual modulations resulting from short-range interactions in primary visual cortex," *Nature (London)* **399**, 655–661 (1999).
63. L. M. Chen, R. M. Friedman, and A. W. R. Aw, "Optical imaging of SI topography in anesthetized and awake squirrel monkey," *J. Neurosci.* **25**, 7648–7659 (2005).
64. S. B. Hofer, T. D. Mrsic-Flogel, T. Bonhoeffer, and M. Hubener, "Lifelong learning: ocular dominance plasticity in mouse visual cortex," *Curr. Opin. Neurobiol.* **16**(4), 451–459 (2006).
65. I. Férézou, S. Bolea, and C. C. Petersen, "Visualizing the cortical representation of whisker touch: voltage-sensitive dye imaging in freely moving mice," *Neuron* **50**(4), 617–629 (2006).
66. D. Attwell and C. Iadecola, "The neural basis of functional brain imaging signals," *TINS* **25**(12), 621–625 (2002).
67. M. Jones, N. Hewson-Stoate, J. Martindale, P. Redgrave, and J. Mayhew, "Nonlinear coupling of neural activity and CBF in rodent barrel cortex," *Neuroimage* **22**(2), 956–965 (2004).
68. S. A. Sheth, M. Nemoto, M. W. Guiou, M. A. Walker, and A. W. Toga, "Spatiotemporal evolution of functional hemodynamic changes and their relationship to neuronal activity," *J. Cereb. Blood Flow Metab.* pp. 1–12 (Mar. 2005).
69. S. Sheth, M. Nemoto, M. Guiou, M. Walker, N. Pouratian, and A. W. Toga, "Evaluation of coupling between optical intrinsic signals and neuronal activity in rat somatosensory cortex," *Neuroimage* **19**(3), 884–894 (2003).
70. J. Martindale, J. Berwick, C. Martin, Y. Kong, Y. Zheng, and J. Mayhew, "Long duration stimuli and nonlinearities in the neural-haemodynamic coupling," *J. Cereb. Blood Flow Metab.* **25**(5), 651–661 (2005).
71. R. D. Hoge, J. Atkinson, B. Gill, G. R. Crelier, S. Marrett, and G. B. Pike, "Investigation of BOLD signal dependence on cerebral blood flow and oxygen consumption: the deoxyhemoglobin dilution model," *Magn. Reson. Med.* **42**, 849–863 (1999).

72. D. A. Boas, G. Strangman, J. P. Culver, R. D. Hoge, G. Jasdzewski, R. A. Poldrack, B. R. Rosen, and J. B. Mandeville, "Can the cerebral metabolic rate of oxygen be estimated with near-infrared spectroscopy?" *Phys. Med. Biol.* **48**(15), 2405–2418 (2003).
73. R. Turner, "How much cortex can a vein drain? Downstream dilution of activation-related cerebral blood oxygenation changes," *Neuroimage* **16**, 1062–1067 (2002).
74. R. B. Buxton, E. C. Wong, and L. R. Frank, "Dynamics of blood flow and oxygenation changes during brain activation: the balloon model," *Magn. Reson. Med.* **39**, 855–864 (1998).
75. J. B. Mandeville, J. J. A. Marota, C. Ayata, G. Zaharchuk, M. A. Moskowitz, B. R. Rosen, and R. M. Weisskoff, "Evidence of a cerebrovascular post-arteriole Windkessel with delayed compliance," *J. Cereb. Blood Flow Metab.* **19**(6), 679–689 (1999).
76. Y. Kong, Y. Zheng, D. Johnston, J. Martindale, M. Jones, S. Billings, and J. Mayhew, "A model of the dynamic relationship between blood flow and volume changes during brain activation," *J. Cereb. Blood Flow Metab.* **24**(12), 1382–1392 (2004).
77. Y. Zheng, D. Johnston, J. Berwick, D. Chen, S. Billings, and J. Mayhew, "A three-compartment model of the hemodynamic response and oxygen delivery to brain," *Neuroimage* **28**(4), 925–939 (2005).
78. Y. Zheng, J. Martindale, D. Johnston, M. Jones, J. Berwick, and J. Mayhew, "A model of the hemodynamic response and oxygen delivery to brain," *Neuroimage* **16**(3, Part 1), 617–637 (2002).
79. D. Kleinfeld, P. P. Mitra, F. Helmchen, and W. Denk, "Fluctuations and stimulus-induced changes in blood flow observed in individual capillaries in layers 2 through 4 of rat neocortex," *Proc. Natl. Acad. Sci. U.S.A.* **95**(26), 15741–15746 (1998).
80. X. Wang, N. Lou, Q. Xu, G. Tian, W. G. Peng, X. Han, J. Kang, T. Takano, and M. Nedergaard, "Astrocytic Ca2+ signaling evoked by sensory stimulation in vivo," *Nat. Neurosci.* **9**(6), 816–823 (2006).
81. A. J. Kennerley, J. Berwick, J. Martindale, D. Johnston, N. Papadakis, and J. E. Mayhew, "Concurrent fMRI and optical measures for the investigation of the hemodynamic response function," *Magn. Reson. Med.* **54**(2), 354–365 (2005).
82. A. F. Cannestra, N. Pouratian, M. H. Shomer, and A. W. Toga, "Refractory periods observed by intrinsic signal and fluorescent dye imaging," *J. Neurophysiol.* **80**(3), 1522–1532 (1998).
83. N. Pouratian, N. Sicotte, D. Rex, N. A. Martin, D. Becker, A. F. Cannestra, and A. W. Toga, "Spatial/temporal correlation of BOLD and optical intrinsic signals in humans," *Nat. Neurosci.* **47**(4), 766–776 (2002).
84. R. S. Menon, S. Ogawa, X. Hu, J. P. Strupp, P. Anderson, and K. Ugurbil, "BOLD based functional MRI at 4 Tesla includes a capillary bed contribution: echo-planar imaging correlates with previous optical imaging using intrinsic signals," *Nat. Neurosci.* **33**(3), 453–459 (1995).
85. D. Malonek, U. Dirnagl, U. Lindauer, K. Yamada, I. Kanno, and A. Grinvald, "Vascular imprints of neuronal activity: relationships between the dynamics of cortical blood flow, oxygenation, and volume changes following sensory stimulation," *Proc. Natl. Acad. Sci. U.S.A.* **94**(26), 14826–14831 (1997).
86. M. Fukuda, P. Wang, C. H. Moon, M. Tanifuji, and S. G. Kim, "Spatial specificity of the enhanced dip inherently induced by prolonged oxygen consumption in cat visual: implication for columnar resolution functional MRIcortex," *Neuroimage* **30**(1), 70–87 (2006).
87. U. Lindauer, G. Royl, C. Leithner, M. Kühl, L. Gold, J. Gethmann, M. Kohl-Bareis, A. Villringer, and U. Dirnagl, "No evidence for early decrease in blood oxygenation in rat whisker cortex in response to functional activation," *Neuroimage* **13**(6), 988–1001 (2001).
88. M. Kohl, C. Nolte, H. R. Heekeren, U. S. S. Horst, H. Obrig, and A. Villringer, "Determination of the wavelength dependence of the differential pathlength factor from near-infrared pulse signals," *Phys. Med. Biol.* **43**, 1771–1782 (1998).
89. R. B. Buxton, "The elusive initial dip," *Neuroimage* **13**(6), 953–958 (2001).
90. A. M. Ba, M. Guiou, N. Pouratian, A. Muthialu, D. E. Rex, A. F. Cannestra, J. W. Y. Chen, and A. W. Toga, "Multiwavelength optical intrinsic signal imaging of cortical spreading depression," *J. Neurophysiol.* **88**, 2726–2735 (2002).
91. H. K. Shin, A. K. Dunn, P. B. Jones, D. A. Boas, M. A. Moskowitz, and C. Ayata, "Vasoconstrictive neurovascular coupling during focal ischemic depolarizations," *J. Cereb. Blood Flow Metab.* **26**(8), 1018–1030 (2005).
92. L. Wei, J. P. Erinjeri, C. M. Rovainen, and T. A. Woolsey, "Collateral growth and angiogenesis around cortical stroke," *Stroke* **32**(9), 2179–2184 (2001).
93. H. K. Shin, S. Salomone, E. M. Potts, S.-W. Lee, E. Millican, K. Noma, P. L. Huang, D. A. Boaz, J. K. Liao, M. A. Moskowitz, and C. Ayata, , "Rho-kinase inhibition acutely augments blood flow in focal cerebral ischemia via endothelial mechanisms," *J. Cereb. Blood Flow Metab.* **27**, 998–1009 (2007).
94. Y. R. Kim, M. P.v.. Meer, J. B. Mandeville, E. Tejima, G. Dai, K. Topalkara, J. Qui, R. M. Dijkhuizen, M. A. Moskowitz, E. H. Lo, and B. R. Rosen, "fMRI of delayed albumin treatment during stroke recovery in rats: implication for fast neuronal habituation in recovering brains," *J. Cereb. Blood Flow Metab.* **27**, 142–153 (2007).
95. J. W. Y. Chen, A. M. O'Farrell, and A. W. Toga, "Optical intrinsic signal imaging in a rodent seizure model," *Neurology* **55**, 312–315 (2000).
96. C. Redecker, G. Hagemann, R. Kohling, H. Straub, O. W. Witte, and E. J. Speckmann, "Optical imaging of epileptiform activity in experimentally induced cortical malformations," *Exp. Neurol.* **192**(2), 288–298 (2005).
97. K. Shibuki, R. Hishida, H. Murakami, M. Kudoh, T. Kawaguchi, M. Watanabe, S. Watanabe, T. Kouuchi, and R. Tanaka, "Dynamic imaging of somatosensory cortical activity in the rat visualized by flavoprotein autofluorescence," *J. Physiol. (London)* **549**(3), 919–927 (2003).
98. K. Shibuki, K. Ono, R. Hishida, and M. Kudoh, "Endogenous fluorescence imaging of somatosensory cortical activities after discrimination learning in rats," *Neuroimage* **30**, 735–744 (2006).
99. K. C. Reinert, R. L. Dunbar, W. Gao, G. Chen, and T. J. Ebner, "Flavoprotein autofluorescence imaging of neuronal activation in the cerebellar cortex in vivo," *J. Neurophysiol.* **92**, 199–211 (2004).
100. B. Weber, C. Burger, M. T. Wyss, G. K. v. Schulthess, F. Scheffold, and A. Buck, "Optical imaging of the spatiotemporal dynamics of cerebral blood flow and oxidative metabolism in the rat barrel cortex," *Eur. J. Neurosci.* **20**, 2664–2670 (2004).
101. M. Tohmi, H. Kitaura, S. Komagata, M. Kudoh, and K. Shibuki, "Enduring critical period plasticity visualized by transcranial flavoprotein imaging in mouse primary visual cortex," *J. Neurosci.* **26**(45), 11775–11785 (2006).
102. K. Takahashi, R. Hishida, Y. Kubota, M. Kudoh, S. Takahashi, and K. Shibuki, "Transcranial fluorescence imaging of auditory cortical plasticity regulated by acoustic environments in mice," *Eur. J. Neurosci.* **23**(5), 1365–1376 (2006).
103. T. Takao, H. Murakami, M. Fukuda, T. Kawaguchi, A. Kakita, H. Takahashi, M. Kudoh, R. Tanaka, and K. Shibuki, "Transcranial imaging of audiogenic epileptic foci in the cortex of DBA/2J mice," *NeuroReport* **17**(3), 267–271 (2006).
104. G. Gratton, C. R. Brumback, B. A. Gordon, M. A. Pearson, K. A. Low, and M. Fabiani, "Effects of measurement method, wavelength, and source-detector distance on the fast optical signal," *Neuroimage* **32**(4), 1576–1590 (2006).
105. J. Steinbrink, F. C. Kempf, A. Villringer, and H. Obrig, "The fast optical signal—robust or elusive when non-invasively measured in the human adult?" *Neuroimage* **26**(4), 996–1008 (2005).
106. L. B. Cohen, R. D. Keynes, and B. Hille, "Light scattering and birefringence changes during nerve activity," *Nature (London)* **218**, 438–441 (1968).
107. D. M. Rector, K. M. Carter, P. L. Volegov, and J. S. George, "Spatio-temporal mapping of rat whisker barrels with fast scattered light signals," *Neuroimage* **26**(2), 619–627 (2005).
108. J. G. Fujimoto, M. E. Brezinski, G. J. Tearney, S. A. Boppart, B. E. Bouma, M. R. Hee, J. F. Southern, and E. A. Swanson, "Optical biopsy and imaging using optical coherence tomography," *Nat. Methods* **1**, 970–972 (1995).
109. R. U. Maheswari, H. Takaoka, H. Kadono, R. Honma, and M. Tanifuji, "Novel functional imaging technique from brain surface with optical coherence tomography enabling visualization of depth resolved functional structure in vivo," *J. Neurosci. Methods* **124**(1), 83–92 (2003).
110. M. Fukuda, U. M. Rajagopalan, R. Homma, M. Matsumoto, M. Nishizaki, and M. Tanifuji, "Localization of activity-dependent changes in blood volume to submillimeter-scale functional domains in cat visual cortex," *Cereb. Cortex* **15**(6), 823–833 (2005).
111. A. D. Aguirre, Y. Chen, J. G. Fujimoto, L. Ruvinskaya, A. Devor, and D. A. Boas, "Depth-resolved imaging of functional activation in

the rat cerebral cortex using optical coherence tomography," *Opt. Lett.* **31**(23), 3459–3461 (2006).
112. E. M. C. Hillman, D. A. Boas, A. M. Dale, and A. K. Dunn, "Laminar optical tomography: demonstration of millimeter-scale depth-resolved imaging in turbid media," *Opt. Lett.* **29**(14), 1650–1652 (2004).
113. E. M. C. Hillman, A. Devor, A. K. Dunn, and D. A. Boas, "Laminar optical tomography: high-resolution 3D functional imaging of superficial tissues," *Proc. SPIE* **6143**, 61431M (2006).
114. J. A. N. Fisher, E. F. Civillico, D. Contreras, and A. G. Yodh, "In vivo fluorescence microscopy of neuronal activity in three dimensions by use of voltage-sensitive dyes," *Opt. Lett.* **29**(1), 71–73 (2004).
115. W. Denk, J. H. Strickler, and W. W. Webb, "Two-photon laser scanning fluorescence microscopy," *Science* **248**(4951), 73–76 (1990).
116. E. Chaigneau, M. Oheim, E. Audinat, and S. Charpak, "Two-photon imaging of capillary blood flow in olfactory bulb glomeruli," *Proc. Natl. Acad. Sci. U.S.A.* **100**(22), 13081–13086 (2003).
117. B. J. Bacskai, G. A. Hickey, J. Skoch, S. T. Kajdasz, Y. Wang, G. F. Huang, C. A. Mathis, W. E. Klunk, and B. T. Hyman, "Four-dimensional multiphoton imaging of brain entry, amyloid binding, and clearance of an amyloid- ligand in transgenic mice," *PNAS* **100**(21), 12462–12467 (2003).
118. K. Svoboda and R. Yasuda, "Principles of two-photon excitation microscopy and its applications to neuroscience," *Neuron* **50**(6), 823–839 (2006).
119. D. Kleinfeld and W. Denk, "Two-photon imaging of neocortical microcirculation," in *Imaging Neurons: A Laboratory Manual*, R. Yuste, F. Lanni, and A. Konnerth, Eds., pp. 2301–2305, Cold Spring Harbor Laboratory Press, New York (1999).
120. D. Kleinfeld and K. R. Delaney, "Distributed representation of vibrissa movement in the upper layers of somatosensory cortex revealed with voltage-sensitive dyes," *J. Comp. Neurol.* **375**, 89–108 (1996).
121. J. T. Trachtenberg, B. E. Chen, G. W. Knott, G. Feng, J. R. Sanes, E. Welker, and K. Svoboda, "Long-term in vivo imaging of experience-dependent synaptic plasticity in adult cortex," *Nature* **420**(6917), 788–794 (2002).
122. T. A. Pologruto, B. L. Sabatini, and K. Svoboda, "ScanImage: flexible software for operating laser scanning microscopes," *Biomed. Eng. Online* **2**(13), (2003).
123. Y. P. Tan, I. Llano, A. Hopt, F. Wurriehausen, and E. Neher, "Fast scanning and efficient photodetection in a simple two-photon microscope," *J. Neurosci. Methods* **92**(1-2), 123–135 (1999).
124. A. Majewska, G. Yiu, and R. Yuste, "A custom-made two-photon microscope and deconvolution system," *Pflugers Arch.* **441**(2-3), 398–408 (2000).
125. P. S. Tsai, N. Nishimura, E. J. Yoder, A. White, E. Dolnick, and D. Kleinfeld, "Principles, design and construction of a two photon scanning microscope for in vitro and in vivo studies," in *Methods for In Vivo Optical Imaging*, R. Frostig, Ed., pp. 113–117, CRC Press, Boca Raton, FL (2002).
126. M. Bouchard, L. Ruvinskaya, D. A. Boas, and E., M. C. Hillman, "Video-rate two-photon microscopy of cortical hemodynamics in-vivo," *BIOMED Proc. OSA Tech. Digest* (2006).
127. K. Ohki, S. Chung, P. Kara, M. Hubener, T. Bonhoeffer, and R. C. Reid, "Highly ordered arrangement of single neurons in orientation pinwheels," *Nature (London)* **24** [442(7105)], 925–928 (2006).
128. A. Villringer, A. Them, U. Lindauer, K. Einhaupl, and U. Dirnagl, "Capillary perfusion of the rat brain cortex. An in vivo confocal microscopy study," *Circ. Res.* **75**(1), 55–62 (1994).
129. E. B. Hutchinson, B. Stefanovic, A. P. Koretsky, and A. C. Silva, "spatial flow-volume dissociation of the cerebral microulatory response to mild hypercapnia," *Neuroimage* **32**(2), 520–530 (2006).
130. H. Liu, T. Kishi, A. G. Roseberry, X. Cai, C. E. Lee, J. M. Montez, J. M. Friedman, and J. K. Elmquist, "Transgenic mice expressing green fluorescent protein under the control of the melanocortin-4 receptor promoter," *J. Neurosci.* **23**, 7143–7154 (2003).
131. S. Pinto, A. G. Roseberry, H. Liu, S. Diano, M. Shanabrough, X. Cai, J. M. Friedman, and T. L. Horvath, "Rapid rewiring of arcuate nucleus feeding circuits by leptin," *Science* **304**(5667), 110–115 (2004).
132. T. Takano, G. Tian, W. Peng, N. Lou, W. Libionka, X. Han, and M. Nedergaard, "Astrocyte-mediated control of cerebral blood flow," *Nat. Neurosci.* **9**, 260–267 (2006).
133. M. Zonta, M. C. Angulo, S. Gobbo, B. Rosengarten, K. A. Hossmann, T. Pozzan, and G. Carmignoto, "Neuron-to-astrocyte signaling is central to the dynamic control of brain microcirculation," *Nat. Neurosci.* **6**(1), 43–50 (2003).
134. J. A. Filosa, A. D. Bonev, and M. T. Nelson, "Calcium dynamics in cortical astrocytes and arterioles during neurovascular coupling," *Circ. Res.* **95**(10), e73–81 (2004).
135. N. Nishimura, C. B. Schaffer, B. Friedman, P. S. Tsai, P. D. Lyden, and D. Kleinfeld, "Targeted insult to subsurface cortical blood vessels using ultrashort laser pulses: three models of stroke," *Nat. Methods* **3**, 99–108 (2006).
136. B. J. Bacskai and B. T. Hyman, "Alzheimer's disease: what multiphoton microscopy teaches us," *Neuroscientist* **8**(5), 386–390 (2002).
137. B. J. Bacskai, S. T. Kajdasz, M. E. McLellan, D. Games, P. Seubert, D. Schenk, and B. T. Hyman, "Non-Fc-mediated mechanisms are involved in clearance of amyloid in vivo by immunotherapy," *J. Neurosci.* **22**(18), 7873–7878 (2002).
138. W. E. Klunk, et al., "Imaging brain amyloid in Alzheimer's disease with Pittsburgh Compound-B," *Ann. Neurol.* **55**(3), 306–319 (2004).
139. J. Skoch, A. Dunn, B. T. Hyman, and B. J. Bacskai, "Development of an optical approach for noninvasive imaging of Alzheimer's disease pathology," *J. Biomed. Opt.* **10**(1), 11007–11014 (2005).
140. B. J. Bacskai, J. Skoch, G. A. Hickey, R. Allen, and B. T. Hyman, "Fluorescence resonance energy transfer determinations using multiphoton fluorescence lifetime imaging microscopy to characterize amyloid-beta plaques," *J. Biomed. Opt.* **8**, 368–375 (2003).
141. K. A. Kasischke, H. D. Vishwasrao, P. J. Fisher, W. R. Zipfel, and W. W. Webb, "Neural activity triggers neuronal oxidative metabolism followed by astrocytic glycolysis," *Science* **305**, 99–103 (2004).
142. D. A. Dombeck, L. Sacconi, M. Blanchard-Desce, and W. W. Webb, "Optical recording of fast neuronal membrane potential transients in acute mammalian brain slices by second-harmonic generation microscopy," *J. Neurophysiol.* **94**(5), 3628–3636 (2005).
143. M. Nuriya, J. Jiang, B. Nemet, K. B. Eisenthal, and R. Yuste, "Imaging membrane potential in dendritic spines," *PNAS* **103**(3), 786–790 (2006).
144. M. A. Franceschini, S. Thaker, G. Themelis, K. K. Krishnamoorthy, H. Bortfeld, S. G. Diamond, D. A. Boas, K. Arvin, and P. E. Grant, "Assessment of infant brain development with frequency-domain near-infrared spectroscopy," *Pediatr. Res.* (in press).
145. J. C. Hebden, et al., "Three-dimensional optical tomography of the premature infant brain," *Phys. Med. Biol.* **47**(23), 4155–4166 (2002).
146. H. Bortfeld, E. Wruck, and D. A. Boas, "Assessing infants' cortical response to speech using near-infrared spectroscopy," *Neuroimage* **34**(1), 407–415 (2007).
147. A. Miki, T. Nakajima, M. Takagi, T. Usui, H. Abe, C. S. Liu, and G. T. Liu, "Near-infrared spectroscopy of the visual cortex in unilateral optic neuritis," *Am. J. Ophthalmol.* **139**(2), 353–356 (2005).
148. M. Igawa, Y. Atsumi, K. Takahashi, S. Shiotsuka, H. Hirasawa, R. Yamamoto, A. Maki, Y. Yamashita, and H. Koizumi, "Activation of visual cortex in REM sleep measured by 24-channel NIRS imaging," *Psychiatry Clin. Neurosci.* **55**(3), 187–188 (2001).
149. A. Obata, K. Morimoto, H. Sato, A. Maki, and H. Koizumi, "Acute effects of alcohol on hemodynamic changes during visual stimulation assessed using 24-channel near-infrared spectroscopy," *Psychiatry Res.* **123**(2), 145–152 (2003).
150. V. Y. Toronov, X. Zhang, and A. G. Webb, "A spatial and temporal comparison of hemodynamic signals measured using optical and functional magnetic resonance imaging during activation in the human primary visual cortex," *Neuroimage* **34**(3), 1136–1148 (2007).
151. M. Bartocci, L. L. Bergqvist, H. Lagercrantz, and K. J. S. Anand, "Pain activates cortical areas in the preterm newborn brain," *Pain* **122**(1-2), 109–117 (2006).
152. M. A. Franceschini, V. Toronov, M. E. Filiaci, E. Gratton, and S. Fantini, "On-line optical imaging of the human brain with 160-ms temporal resolution," *Opt. Express* **6**(3), 49–57 (2000).
153. M. A. Franceschini, S. Fantini, J. H. Thompson, J. P. Culver, and D. A. Boas, "Hemodynamic evoked response of the sensorimotor cortex measured non-invasively with near-infrared optical imaging," *Psychophysiology* **40**, 548–560 (2003).
154. M. Tanosaki, Y. Hoshi, Y. Iguchi, Y. Oikawa, I. Oda, and M. Oda, "Variation of temporal characteristics in human cerebral hemody-

namic responses to electric median nerve stimulation: a near-infrared spectroscopic study," *Neurosci. Lett.* **316**(2), 75–78 (2001).
155. M. J. Herrmann, A. C. Ehlis, A. Wagener, C. P. Jacob, and A. J. Fallgatter, "Near-infrared optical topography to assess activation of the parietal cortex during a visuo-spatial task," *Neuropsychologia* **43**(12), 1713–1720 (2005).
156. A. Jayakar, C. Dunoyer, G. Rey, I. Yaylali, and P. Jayakar, "Near-infrared spectroscopy to define cognitive frontal lobe functions," *J. Clin. Neurophysiol.* **22**(6), 415–417 (2005).
157. T. Wilcox, H. Bortfeld, R. Woods, E. Wruck, and D. A. Boas, "Using near-infrared spectroscopy to assess neural activation during object processing in infants," *J. Biomed. Opt.* **10**(1), 11010 (2005).
158. H. Harada, M. Tanaka, and T. Kato, "Brain olfactory activation measured by near-infrared spectroscopy in humans," *J. Laryngol. Otol.* **120**(8), 638–643 (2006).
159. T. J. Huppert, R. D. Hoge, S. G. Diamond, M. A. Franceschini, and D. A. Boas, "A temporal comparison of BOLD, ASL, and NIRS hemodynamic responses to motor stimuli in adult humans," *Neuroimage* **29**(2), 368–382 (2006).
160. R. D. Hoge, M. A. Franceschini, R. J. Covolan, T. Huppert, J. B. Mandeville, and D. A. Boas, "Simultaneous recording of task-induced changes in blood oxygenation, volume, and flow using diffuse optical imaging and arterial spin-labeling MRI," *Neuroimage* **25**(3), 701–707 (2005).
161. K. A. Low, E. Leaver, A. F. Kramer, M. Fabiani, and G. Gratton, "Fast optical imaging of frontal cortex during active and passive oddball tasks," *Psychophysiology* **43**(2), 127–136 (2006).
162. B. M. Mackert, G. Wubbeler, S. Leistner, K. Uludag, H. Obrig, A. Villringer, L. Trahms, and G. Curio, "Neurovascular coupling analyzed non-invasively in the human brain," *NeuroReport* **15**(1), 63–66 (2004).
163. S. Kahraman, H. Kayali, C. Atabey, F. Acar, and S. Gocmen, "The accuracy of near-infrared spectroscopy in detection of subdural and epidural hematomas," *J. Trauma* **61**(6), 1480–1483 (2006).
164. G. Strangman, R. Goldstein, S. L. Rauch, and J. Stein, "Near-infrared spectroscopy and imaging for investigating stroke rehabilitation: test-retest reliability and review of the literature," *Arch. Phys. Med. Rehabil.* **87**(12), 12–19 (2006).
165. G. Leyvi, R. Bello, J. D. Wasnick, and K. Plestis, "Assessment of cerebral oxygen balance during deep hypothermic circulatory arrest by continuous jugular bulb venous saturation and near-infrared spectroscopy," *J. Cardiothorac Vasc. Anesth.* **20**(6), 826–833 (2006).
166. L. A. Nelson, J. C. McCann, A. W. Loepke, J. Wu, B. B. Dor, and C. D. Kurth, "Development and validation of a multiwavelength spatial domain near-infrared oximeter to detect cerebral hypoxia-ischemia," *J. Biomed. Opt.* **11**(6), 064022 (2006).
167. Q. Zhang, H. Ma, S. Nioka, and B. Chance, "Study of near infrared technology for intracranial hematoma detection," *J. Biomed. Opt.* **5**(2), 206–213 (2000).
168. R. Springett, Y. Sakata, and D. T. Delpy, "Precise measurement of cerebral blood flow in newborn piglets from the bolus passage of indocyanine green," *Phys. Med. Biol.* **46**(8), 2209–2225 (2001).
169. Z. Bashir, J. Miller, J. A. Miyan, and M. S. Thorniley, "A near infrared spectroscopy study investigating oxygen utilisation in hydrocephalic rats," *Exp. Brain Res.* **175**(1), 127–138 (2006).
170. H. E. D'Arceuil, M. P. Hotakainen, C. Liu, G. Themelis, A. J. D. Crespigny, and M. A. Franceschini, "Near-infrared frequency-domain optical spectroscopy and magnetic resonance imaging: a combined approach to studying cerebral maturation in neonatal rabbits," *J. Biomed. Opt.* **10**(1), 11011 (2005).
171. E. A. Berker, A. H. Berker, and A. Smith, "Translation of Broca's 1865 report. Localization of speech in the third left frontal convolution," *Arch. Neurol.* **43**, 1065–1072 (1986).
172. S. Zago, M. Nurra, G. Scarlato, and V. Silani, "Bartolomeo Panizza and the discovery of the brain's visual center," *Arch. Neurol.* **57**(11), 1642–1648 (2000).
173. Y. Xu, H. L. Graber, and R. L. Barbour, "Image correction algorithm for functional three-dimensional diffuse optical tomography brain imaging," *Appl. Opt.* **46**(10), 1693–1704 (2007).
174. A. Bluestone, G. Abdoulaev, C. Schmitz, R. Barbour, and A. Hielsher, "Three dimensional optical tomography of hemodynamics in the human head," *Opt. Express* **9**(6), 272–286 (2001).
175. D. A. Boas, K. Chen, D. Grebert, and M. A. Franceschini, "Improving the diffuse optical imaging spatial resolution of the cerebral hemodynamic response to brain activation in humans," *Opt. Lett.* **29**(13), 1506–1508 (2004).
176. J. P. Culver, B. L. Schlaggar, H. Dehghani, and B. W. Zeff, "Diffuse optical tomography for mapping human brain function," *Proc. IEEE LSSA Workshop*, pp. 122–123 (2006).
177. C. H. Schmitz, M. Löcker, J. Lasker, A. H. Hielsher, and R. L. Barbour, "Instrumentation for fast functional optical tomography," *Rev. Sci. Instrum.* **73**(2), 429–439 (2002).
178. Y. Yamashita, A. Maki, and H. Koizumi, "Near-infra-red topographic measurement system: Imaging of absorbers localized in a scattering medium," *Rev. Sci. Instrum.* **67**(3), 730–732 (1996).
179. D. K. Joseph, T. J. Huppert, M. A. Franceschini, and D. A. Boas, "Diffuse optical tomography system to image brain activation with improved spatial resolution and validation with functional magnetic resonance imaging," *Appl. Opt.* **45**(31), 8142–8151 (2006).
180. M. A. Franceschini, D. K. Joseph, T. J. Huppert, S. G. Diamond, and D. A. Boas, "Diffuse optical imaging of the whole head," *J. Biomed. Opt.* **11**, 054007 (2006).
181. N. L. Everdell, A. P. Gibson, I. D. C. Tullis, T. Vaithianathan, J. C. Hebden, and D. T. Delpy, "A frequency multiplexed near infrared topography system for imaging functional activation in the brain," *Rev. Sci. Instrum.* **76**, 093705 (2005).
182. I. Nissila, et al., "Comparison between a time-domain and a frequency-domain system for optical tomography," *J. Biomed. Opt.* **11**(6), 064015 (2006).
183. D. M. Hueber, M. A. Franceschini, H. Y. Ma, Q. Zhang, J. R. Ballesteros, S. Fantini, D. Wallace, V. Ntziachristos, and B. Chance, Non-invasive and quantitative near-infrared haemoglobin spectrometry in the piglet brain during hypoxic stress, using a frequency-domain multidistance instrument," *Phys. Med. Biol.* **46**, 41–62 (2001).
184. V. Ntziachristos, X. Ma, A. G. Yodh, and B. Chance, "Multichannel photon counting instrument for spatially resolved near infrared spectroscopy," *Rev. Sci. Instrum.* **70**(1), 193–201 (1999).
185. J. Selb, D. K. Joseph, and D. A. Boas, "Time-gated optical system for depth-resolved functional brain imaging," *J. Biomed. Opt.* **11**(4), 044008 (2006).
186. F. E. W. Schmidt, M. E. Fry, E. M. C. Hillman, J. C. Hebden, and D. T. Delpy, "A 32-channel time-resolved instrument for medical optical tomography," *Rev. Sci. Instrum.* **71**(1), 256–265 (2000).
187. J. Steinbrink, H. Wabnitz, H. Obrig, A. Villringer, and H. Rinneberg, "Determining changes in NIR absorption using a layered model of the human head," *Phys. Med. Biol.* **46**, 879–896 (2001).
188. B. Montcel, R. Chabrier, and P. Poulet, "Detection of cortical activation with time-resolved diffuse optical methods," *Appl. Opt.* **44**(10), 1942–1947 (2005).
189. T. Vaithianathan, I. D. C. Tullis, N. Everdell, T. Leung, A. Gibson, J. Meek, and D. T. Delpy, "Design of a portable near infrared system for topographic imaging of the brain in babies," *Rev. Sci. Instrum.* **75**, 3276–3283 (2004).
190. D. T. Delpy, M. Cope, P. v. d. Zee, S. Arridge, S. Wray, and J. S. Wyatt, "Estimation of optical pathlength through tissue from direct time of flight measurement," *Phys. Med. Biol.* **33**(12), 1433–1442 (1988).
191. I. D. C. Tullis and D. T. Delpy, "An optical pathlength meter for near infrared spectroscopy," *Proc. SPIE* **4432**, 17–23 (2001).
192. D. A. Boas, J. P. Culver, J. J. Stott, and A. K. Dunn, "Three dimensional Monte Carlo code for photon migration through complex heterogeneous media including the adult human head," *Opt. Express* **10**, 159–170 (2002).
193. A. Custo, W. M. Wells, A. H. Barnett, E. M. C. Hillman, and D. A. Boas, "Effective scattering coefficient of the cerebral spinal fluid in adult head models for diffuse optical imaging," *Appl. Opt.* **45**(19), 4747–4755 (2006).
194. T. Koyama, A. Iwasaki, Y. Ogoshi, and E. Okada, "Practical and adequate approach to modeling light propagation in an adult head with low-scattering regions by use of diffusion theory," *Appl. Opt.* **44**(11), 2094–2103 (2005).
195. J. Heiskala, I. Nissila, T. Neuvonen, S. Jarvenpaa, and E. Somersalo, "Modeling anisotropic light propagation in a realistic model of the human head," *Appl. Opt.* **44**(11), 2049–2057 (2005).
196. Y. Fukui, Y. Ajichi, and E. Okada, "Monte Carlo prediction of near-infrared light propagation in realistic adult and neonatal head models," *Appl. Opt.* **42**(16), 2881–2887 (2003).

197. S. R. Arridge, M. Cope, and D. T. Delpy, "The theoretical basis for the determination of optical pathlengths in tissue: temporal and frequency analysis," *Phys. Med. Biol.* **37**, 1531–1559 (1992).
198. M. Firbank, E. Okada, and D. T. Delpy, "A theoretical study of the signal contribution of regions of the adult head to near infrared spectroscopy studies of visual evoked responses," *Neuroimage* **8**, 69–78 (1998).
199. H. Dehghani, S. R. Arridge, M. Schweiger, and D. T. Delpy, "Optical tomography in the presence of void regions," *J. Opt. Soc. Am. A* **17**(9), 1659–1670 (2000).
200. P. van-der-Zee, Measurement and modelling of the optical properties of human tissue in the near infrared," in *Department of Medical Physics and Bioengineering*, p. 313, University College London, London (1992).
201. A. H. Barnett, J. P. Culver, A. G. Sorensen, A. Dale, and D. A. Boas, "Robust inference of baseline optical properties of the human head with three-dimensional segmentation from magnetic resonance imaging," *Appl. Opt.* **42**, 3095–3108 (2003).
202. D. A. Boas and A. M. Dale, "Simulation study of magnetic resonance imaging-guided cortically constrained diffuse optical tomography of human brain function," *Appl. Opt.* **44**(10), 1957–1968 (2005).
203. A. Liebert, H. Wabnitz, J. Steinbrink, H. Obrig, M. Möller, R. Macdonald, A. Villringer, and H. Rinneberg, "Time-resolved multidistance near-infrared spectroscopy of the adult head: intracerebral and extracerebral absorption changes from moments of distribution of times of flight of photons," *Appl. Opt.* **43**, 3037–3047 (2004).
204. G. Strangman, M. A. Franceschini, and D. A. Boas, "Factors affecting the accuracy of near-infrared spectroscopy concentration calculations for focal changes in oxygenation parameters," *Neuroimage* **18**(4), 865–879 (2003).
205. G. Strangman, J. P. Culver, J. H. Thompson, and D. A. Boas, "A quantitative comparison of simultaneous BOLD fMRI and NIRS recordings during functional brain activation," *Neuroimage* **17**(2), 719–731 (2002).
206. M. Firbank, C. E. Elwell, C. E. Cooper, and D. T. Delpy, "Experimental and theoretical comparison of NIR spectroscopy measurements of cerebral hemoglobin changes," *J. Appl. Physiol.* **85**(5), 1915–1921 (1998).
207. I. Tachtsidis, C. E. Elwell, T. S. Leung, C. W. Lee, M. Smith, and D. T. Delpy, "Investigation of cerebral haemodynamics by near infrared spectroscopy in young healthy volunteers reveals posture dependent spontaneous oscillations," *Physiol. Meas* **25**(2), 437–445 (2004).
208. C. E. Elwell, R. Springett, E. M. C. Hillman, and D. T. Delpy, "Oscillations in cerebral haemodynamics—implications for functional activation studies," *Adv. Exp. Med. Biol.* **471**, 57–65 (1999).
209. H. Obrig, M. Neufang, R. Wenzel, M. Kohl, J. Steinbrink, K. Einhaupl, and A. Villringer, "Spontaneous low frequency oscillations of cerebral hemodynamics and metabolism in human adults," *Neuroimage* **12**(6), 623–639 (2000).
210. J. E. W. Mayhew, S. Askew, Y. Zheng, J. Porrill, G. W. M. Westby, P. Redgrave, D. M. Rector, and R. M. Harper, "Cerebral vasomotion: a 0.1-Hz oscillation in reflected light imaging of neural activity," *Neuroimage* **4**, 183–193 (1996).
211. S. Boden, H. Obrig, C. Kohncke, H. Benav, S. P. Koch, and J. Steinbrink, "The oxygenation response to functional stimulation: Is there a physiological meaning to the lag between parameters?" *Neuroimage* **36**(1), 100–107 (2007).
212. J. Selb, J. J. Stott, M. A. Franceschini, A. G. Sorensen, and D. A. Boas, "Improved sensitivity to cerebral hemodynamics during brain activation with a time-gated optical system: analytical model and experimental validation," *J. Biomed. Opt.* **10**(1), 11013 (2005).
213. S. G. Diamond, T. J. Huppert, V. Kolehmainen, M. A. Franceschini, J. P. Kaipio, S. R. Arridge, and D. A. Boas, "Dynamic physiological modeling for functional diffuse optical tomography," *Neuroimage* **30**(1), 88–101 (2006).
214. S. Prince, V. Kolehmainen, J. P. Kaipio, M. A. Franceschini, D. A. Boas, and S. R. Arridge, "Time-series estimation of biological factors in optical diffusion tomography," *Phys. Med. Biol.* **48**, 1491–1504 (2003).
215. S. R. Arridge, "Optical tomography in medical imaging," *Inverse Probl.* **15**, 41–93 (1999).
216. H. Kawaguchi, T. Hayashi, T. Kato, and E. Okada, "Theoretical evaluation of accuracy in position and size of brain activity obtained by near-infrared topography," *Phys. Med. Biol.* **49**(12), 2753–2765 (2004).
217. E. M. C. Hillman, "Experimental and theoretical investigations of near infrared tomographic imaging methods and clinical applications," PhD Thesis, *Department of Medical Physics and Bioengineering, University College*, University of London: London (2002).
218. V. Ntziachristos, B. Chance, and A. G. Yodh, "Differential diffuse optical tomography," *Opt. Express* **5**, 230–242 (1999).
219. E. M. C. Hillman, H. Dehghani, J. C. Hebden, S. R. Arridge, M. Schweiger, and D. T. Delpy, "Differential imaging in heterogeneous media: limitations of linearization assumptions in optical tomography," *Proc. SPIE* **4250**, 327–338 (2001).
220. G. Gratton and P. M. Corballis, "Removing the heart from the brain: compensation for the pulse artifact in the photon migration signal," *Psychophysiology* **32**(3), 292–299 (1995).
221. S. R. Hintz, D. A. Benaron, J. P. v. Houten, J. L. Duckworth, F. W. H. Liu, S. D. Spilman, D. K. Stevenson, and W. F. Cheong, "Stationary headband for clinical time-of-flight optical imaging at the bedside," *Photochem. Photobiol.* **68**, 361–369 (1998).
222. A. P. Gibson, T. Austin, N. L. Everdell, M. Schweiger, S. R. Arridge, J. H. Meek, J. S. Wyatt, D. T. Delpy, and J. C. Hebden, "Three-dimensional whole-head optical tomography of passive motor evoked responses in the neonate," *Neuroimage* **30**(2), 521–528 (2006).
223. T. Austin, A. P. Gibson, G. Branco, R. Yusof, S. R. Arridge, J. H. Meek, J. S. Wyatt, D. T. Delpy, and J. C. Hebden, "Three-dimensional optical imaging of blood volume and oxygenation in the preterm brain," *Neuroimage* **31**, 1426–1433 (2006).
224. T. D. Yates, J. C. Hebden, A. P. Gibson, N. L. Everdell, S. R. Arridge, and M. Douek, "Optical tomography of the breast using a multi-channel time-resolved imager," *Phys. Med. Biol.* **50**, 2503–2517 (2005).
225. E. M. C. Hillman, J. C. Hebden, M. Schweiger, H. Dehghani, F. E. W. Schmidt, D. T. Delpy, and S. R. Arridge, "Time resolved optical tomography of the human forearm," *Phys. Med. Biol.* **46**(4), 1117–1130 (2001).
226. E. M. C. Hillman, J. C. Hebden, F. E. W. Schmidt, S. R. Arridge, M. Schweiger, H. Dehghani, and D. T. Delpy, "Calibration techniques and datatype extraction for time-resolved optical tomography," *Rev. Sci. Instrum.* **71**(9), 3415–3427 (2000).
227. S. R. Arridge and W. R. B. Lionheart, "Nonuniqueness in diffusion-based optical tomography," *Opt. Lett.* **23**, 882–884 (1998).
228. A. Corlu, R. Choe, T. Durduran, K. Lee, M. Schweiger, S. R. Arridge, E. M. C. Hillman, and A. G. Yodh, "Diffuse optical tomography with spectral constraints and wavelength optimization," *Appl. Opt.* **44**(11), 2082–2093 (2005).
229. J. C. Hebden, F. E. W. Schmidt, M. E. Fry, M. Schweiger, E. M. C. Hillman, and D. T. Delpy, "Simultaneous reconstruction of absorption and scattering images by multichannel measurement of purely temporal data," *Opt. Lett.* **24**, 534–536 (1999).
230. A. Gibson, et al., "Optical tomography of a realistic neonatal head phantom," *Appl. Opt.* **42**, 3109–3116 (2003).
231. A. P. Gibson, J. Riley, M. Schweiger, J. C. Hebden, S. R. Arridge, and D. D. T. Delpy, "A method for generating patient-specific finite element meshes for head modelling," *Phys. Med. Biol.* **48**, 481–495 (2003).
232. M. Schweiger, "Application of the finite element method in infrared image reconstruction of scattering media," in *Department of Medical Physics and Bioengineering*, *University College*, University of London, London (1994).
233. M. Schweiger, S. R. Arridge, and I. Nissilä, "Gauss-Newton method for image reconstruction in diffuse optical tomography," *Phys. Med. Biol.* **50**, 2365–2386 (2005).
234. T. O. Mcbride, B. W. Pogue, S. Jiang, U. L. Österberg, K. D. Paulsen, and S. P. Poplack, "Multi-spectral near-infrared tomography: a case study in compensating for water and lipid content in hemoglobin imaging of the breast," *J. Biomed. Opt.* **7** (1), 72–80 (2002).
235. T. J. Huppert, R. D. Hoge, A. M. Dale, M. A. Franceschini, and D. A. Boas, "Quantitative spatial comparison of diffuse optical imaging with blood oxygen level-dependent and arterial spin labeling-based functional magnetic resonance imaging," *J. Biomed. Opt.* **11**(6), 064018 (2006).
236. H. Dehghani, see: http://biolight.thayer.dartmouth.edu/TomoPage.html.

237. D. A. Boas, T. Gaudette, and S. R. Arridge, "Simultaneous imaging and optode calibration with diffuse optical tomography," *Opt. Express* **8**(5), 263–270 (2001).
238. J. C. Hebden, A. Gibson, T. Austin, R. Yusof, N. Everdell, D. T. Delpy, S. R. Arridge, J. H. Meek, and J. S. Wyatt, "Imaging changes in blood volume and oxygenation in the newborn infant brain using three-dimensional optical tomography," *Phys. Med. Biol.* **49**, 1117–1130 (2004).
239. D. T. Delpy, see: http://www.medphys.ucl.ac.uk/research/borl/research/NIRtopics/spectra/spectra.htm.
240. C. E. Cooper and R. Springett, "Measurement of cytochrome oxidase and mitochondrial energetics by near-infrared spectroscopy," *Philos. Trans. R. Soc. London, Ser. B* **352**(1354), 669–676 (1997).
241. C. E. Cooper, et al., "Measurement of cytochrome oxidase redox state by near infrared spectroscopy," *Adv. Exp. Med. Biol.* **413**, 63–73 (1997).
242. R. Springett, J. Newman, M. Cope, and D. T. Delpy, "Oxygen dependency and precision of cytochrome oxidase signal from full spectral NIRS of the piglet brain," *Am. J. Physiol. Heart Circ. Physiol.* **279**(5), H2202–2209 (2000).
243. A. D. McGown, H. Makker, C. Elwell, P. G. A. Rawi, A. Valipour, and S. G. Spiro, "Measurement of changes in cytochrome oxidase redox state during obstructive sleep apnea using near-infrared spectroscopy," *Sleep* **26**(6), 1–7 (2003).
244. A. R. A. Salam, G. B. Drummond, H. W. Bauld, and D. B. Scott, "Clearance of indocyanine green as an index of liver function during cyclopropane anaesthesia and induced hypotension," *Br. J. Anaesth.* **48**(3), 231–238 (1976).
245. F. Gora, S. Shinde, C. E. Elwell, J. C. Goldstone, M. Cope, D. T. Delpy, and M. Smith, "Measurement of cerebral blood flow in adults using near infrared spectroscopy and indocyanine green," *J. Neurosurg. Anesthesiol.* **14**, 218–222 (2002).
246. A. Liebert, H. Wabnitz, J. Steinbrink, M. Moller, R. Macdonald, H. Rinneberg, A. Villringer, and H. Obrig, "Bed-side assessment of cerebral perfusion in stroke patients based on optical monitoring of a dye bolus by time-resolved diffuse reflectance," *Neuroimage* **24**(2), 426–435 (2005).
247. T. S. Leung, A. Narendra, C. E. Elwell, D. T. Delpy, and K. Costeloe, "A new method for the measurement of cerebral blood volume and total circulating blood volume using near infrared spatially resolved spectroscopy and indocyanine green: application and validation in neonates," *Pediatr. Res.* **55**(1), 134–141 (2004).
248. A. Liebert, H. Wabnitz, H. Obrig, R. Erdmann, M. Moller, R. Macdonald, H. Rinneberg, A. Villringer, and J. Steinbrink, "Noninvasive detection of fluorescence from exogenous chromophores in the adult human brain," *Neuroimage* **31**(2), 600–608 (2006).
249. R. Weissleder, "A clearer vision for in vivo imaging," *Nat. Biotechnol.* **19**(4), 316–317 (2001).
250. G. Gratton, M. Fabiani, P. M. Corballis, D. C. Hood, M. R. Goodman-Wood, J. Hirsch, K. Kim, D. Friedman, and E. Gratton, "Fast and localized event-related optical signals (EROS) in the human occipital cortex: comparisons with the visual evoked potential and fMRI," *Neuroimage* **6**(3), 168–180 (1997).
251. M. A. Franceschini and D. A. Boas, "Noninvasive measurement of neuronal activity with near-infrared optical imaging," *Neuroimage* **21**(1), 372–386 (2004).
252. J. P. Culver, T. Durduran, D. Furuya, C. Cheung, J. H. Greenberg, and A. G. Yodh, "Diffuse optical tomography of cerebral blood flow, oxygenation, and metabolism in rat during focal ischemia," *J. Cereb. Blood Flow Metab.* **23**(8), 911–924 (2003).
253. D. A. Boas, L. E. Campbell, and A. G. Yodh, "Scattering and imaging with diffusing temporal field correlations," *Phys. Rev. Lett.* **75**(9), 1855–1858 (1995).
254. D. A. Boas and A. G. Yodh, "Spatially varying dynamical properties of turbid media probed with diffusing temporal light correlation," *J. Opt. Soc. Am. A* **14**, 192–215 (1997).
255. T. Durduran, G. Yu, M. G. Burnett, J. A. Detre, J. H. Greenberg, J. Wang, C. Zhou, and A. G. Yodh, "Diffuse optical measurement of blood flow, blood oxygenation, and metabolism in a human brain during sensorimotor cortex activation," *Opt. Lett.* **29**(15), 1766–1768 (2004).
256. C. Zhou, G. Yu, F. Daisuke, J. H. Greenberg, A. G. Yodh, and T. Durduran, "Diffuse optical correlation tomography of cerebral blood flow during cortical spreading depression in rat brain," *Opt. Express* **14**, 1125–1144 (2006).
257. S. A. Prahl, see http://omlc.ogi.edu/spectra/hemoglobin/summary.html.